



Swansea University
Prifysgol Abertawe



Cronfa - Swansea University Open Access Repository

This is an author produced version of a paper published in:
Computer Methods in Applied Mechanics and Engineering

Cronfa URL for this paper:

<http://cronfa.swan.ac.uk/Record/cronfa39597>

Paper:

Ortigosa, R., Franke, M., Janz, A., Gil, A. & Betsch, P. (2018). An energy–momentum time integration scheme based on a convex multi-variable framework for non-linear electro-elastodynamics. *Computer Methods in Applied Mechanics and Engineering*

<http://dx.doi.org/10.1016/j.cma.2018.04.021>

This item is brought to you by Swansea University. Any person downloading material is agreeing to abide by the terms of the repository licence. Copies of full text items may be used or reproduced in any format or medium, without prior permission for personal research or study, educational or non-commercial purposes only. The copyright for any work remains with the original author unless otherwise specified. The full-text must not be sold in any format or medium without the formal permission of the copyright holder.

Permission for multiple reproductions should be obtained from the original author.

Authors are personally responsible for adhering to copyright and publisher restrictions when uploading content to the repository.

<http://www.swansea.ac.uk/library/researchsupport/ris-support/>

Accepted Manuscript

An energy–momentum time integration scheme based on a convex multi-variable framework for non-linear electro-elastodynamics

R. Ortigosa, M. Franke, A. Janz, A.J. Gil, P. Betsch

PII: S0045-7825(18)30200-7
DOI: <https://doi.org/10.1016/j.cma.2018.04.021>
Reference: CMA 11872

To appear in: *Comput. Methods Appl. Mech. Engrg.*

Received date: 6 February 2018
Revised date: 12 April 2018
Accepted date: 13 April 2018

Please cite this article as: R. Ortigosa, M. Franke, A. Janz, A.J. Gil, P. Betsch, An energy–momentum time integration scheme based on a convex multi-variable framework for non-linear electro-elastodynamics, *Comput. Methods Appl. Mech. Engrg.* (2018), <https://doi.org/10.1016/j.cma.2018.04.021>

This is a PDF file of an unedited manuscript that has been accepted for publication. As a service to our customers we are providing this early version of the manuscript. The manuscript will undergo copyediting, typesetting, and review of the resulting proof before it is published in its final form. Please note that during the production process errors may be discovered which could affect the content, and all legal disclaimers that apply to the journal pertain.



An energy-momentum time integration scheme based on a convex multi-variable framework for non-linear electro-elastodynamics

R. Ortigosa^{†1}, M. Franke^{‡2}, A. Janz[‡], A. J. Gil^{†3}, P. Betsch[‡]

[†]Zienkiewicz Centre for Computational Engineering, College of Engineering
Swansea University, Bay Campus, SA1 8EN, United Kingdom

[‡]Institute of Mechanics, Karlsruhe Institute of Technology
76131 Karlsruhe, Germany

Abstract

This paper introduces a new one-step second order accurate energy-momentum (EM) preserving time integrator for reversible electro-elastodynamics. The new scheme is shown to be extremely useful for the long-term simulation of electroactive polymers (EAPs) undergoing massive strains and/or electric fields. The paper presents the following main novelties. (1) The formulation of a new energy momentum time integrator scheme in the context of nonlinear electro-elastodynamics. (2) The consideration of well-posed *ab initio* convex multi-variable constitutive models. (3) Based on the use of alternative mixed variational principles, the paper introduces two different EM time integration strategies (one based on the Helmholtz's and the other based on the internal energy). (4) The new time integrator relies on the definition of four discrete derivatives of the internal/Helmholtz energies representing the algorithmic counterparts of the work conjugates of the right Cauchy-Green deformation tensor, its co-factor, its determinant and the Lagrangian electric displacement field. (5) Proof of thermodynamic consistency and of second order accuracy with respect to time of the resulting algorithm is included. Finally, a series of numerical examples are included in order to demonstrate the robustness and conservation properties of the proposed scheme, specifically in the case of long-term simulations.

Keywords: electroactive polymer, electro-elastodynamics, multi-variable convexity, energy-momentum scheme.

1. Introduction

Electro Active Polymers (EAPs) [41, 40, 42, 29] represent an important family of smart materials where dielectric elastomers and piezoelectric polymers are some of their most iconic integrants. Dielectric elastomers are very well-known for their outstanding actuation capabilities and low stiffness properties, which makes them ideal for their use as *soft robots* [35]. For instance, electrically induced area expansions of over 380% on dielectric elastomer thin films placed on the verge of snap-through configurations have been reported by Li et al. [30]. Other applications for dielectric elastomers include Braille displays, deformable lenses, haptic devices and energy generators, to name but a few. [14]. Piezoelectric polymers have similar dielectric properties to dielectric elastomers but, on the other hand, have much larger stiffness. As a result, piezoelectric polymers cannot in principle exhibit large electrically induced deformations. Instead, they can be used as moderately deformable actuators. Other important type of applications for these materials include tactile sensors, energy harvesters, acoustic transducers and inertial sensors [35, 14].

¹Corresponding author: r.ortigosa@swansea.ac.uk

²Corresponding author: marlon.franke@kit.edu@kit

³Corresponding author: a.j.gil@swansea.ac.uk

1 The variational formulation of the governing equations of these materials is well established.
 2 In the most standard formulation, displacements and the scalar electric potential [51, 52, 53, 28,
 3 50, 17, 51] are modelled as the unknown fields. In this formulation, the constitutive information is
 4 encapsulated in the Helmholtz energy functional via its invariant-based representation depending
 5 upon kinematic strain measures and the electric field [13, 12]. However, for more complex consti-
 6 tutive models than that of an ideal dielectric elastomer, the saddle point nature of the Helmholtz
 7 functional (convex with respect to the deformation gradient tensor and concave with respect to
 8 the electric field in the small strain/small electric field regime), makes in general impossible to
 9 define *a priori* constitutive models which satisfy the ellipticity condition [31, 5, 47, 46]. This is
 10 a necessary condition that ensures the well-posedness of the problem. Motivated by the possible
 11 loss of ellipticity of the Helmholtz functional, Gil and Ortigosa [20, 37, 36] advocated for the use
 12 of the internal energy functional for the definition of constitutive models in nonlinear electro-
 13 mechanics. In essence, the authors postulated a definition of the internal energy convex with
 14 respect to an extended set of arguments, namely the deformation gradient tensor \mathbf{F} , its co-factor
 15 \mathbf{H} , its Jacobian J , the Lagrangian electric displacement field \mathbf{D}_0 and \mathbf{d} , defined as $\mathbf{d} = \mathbf{F}\mathbf{D}_0$
 16 and proved that this definition satisfies the ellipticity condition unconditionally. Crucially, it is
 17 then possible to safely introduce the Helmholtz energy via a Legendre transformation.
 18

19 The objective of this paper is to derive a new and robust EM time integrator scheme, tailor-
 20 made for nonlinear electro-elastodynamics [48, 21]. The proposed time integrator is extremely
 21 suitable for long-term numerical simulations of EAPs in both actuation and energy harvesting
 22 scenarios. An example that showcases the applicability of the method in actuation scenarios is
 23 the consideration of EAP-based actuators subjected to a time dependent electric field in order to
 24 achieve user-defined operational configurations.
 25

26 Consistent implicit EM time integration schemes (EM schemes in the sequel) inherit the
 27 conservation laws of total energy, linear momentum and angular momentum. The *consistency* of
 28 these types of algorithms refer to their ability to preserve or dissipate the total energy of a system
 29 in agreement with the laws of thermodynamics [23], hence not restricting their applicability to
 30 (reversible) hyperelastic isotropic material models. For instance, EM consistent integrators can
 31 also be applied in the context of mixed variational formulations [7], anisotropic material behaviour
 32 [25], non-linear visco-elastodynamics [23, 32] and non-linear elasto-thermodynamics [26, 19]. A
 33 great overview of the development of EM schemes is provided by the textbook [6].
 34

35 In the purely mechanical case, the thermodynamical consistency of these methods is ensured
 36 by virtue of replacing the (exact) derivative of the strain energy with respect to the right Cauchy-
 37 Green deformation tensor (i.e. the consistent second Piola-Kirchhoff stress tensor) with its algo-
 38 rithmic counterpart. The latter, denoted as discrete derivative [21, 19, 7, 44] must be defined in
 39 compliance with the so-called *directionality property*. Specially interesting is the recent work by
 40 Betsch et al. [8], where a new consistent EM time integrator scheme has been developed in the
 41 context of polyconvex elasticity. Essentially, these authors proposed the consideration of three
 42 discrete derivatives of the strain energy (as opposed to the single discrete derivative used in the
 43 standard case). Each discrete derivative represents the algorithmic counterpart of the work conju-
 44 gates of the right Cauchy-Green deformation tensor, its co-factor and its determinant. In a recent
 45 work [19], this formulation has been extended to the field of thermo-elasticity. In comparison to
 46 previously proposed discrete derivative expressions (see e.g. [21, 24]), the new stress formula in
 47 [8, 19] assumes a remarkably simple form. A key factor for that simplification is the use of a
 48 tensor cross product pioneered by the Boer [15] and employed for the first time by Bonet et. al.
 49 [9, 10] in the case of nonlinear electromechanics [20, 37, 36, 38].
 50

51 The outline of this paper is as follows: in Section 2, some basic principles of kinematics are
 52 presented. The governing equations in nonlinear electro-elastodynamics are also presented in this
 53 section. The concept of multi-variable convexity and its importance from the material stability
 54 point of view is presented in Section 3. Section 4 starts with the three-field mixed formulation
 55
 56
 57
 58
 59
 60
 61
 62
 63
 64
 65

presented in Reference [20] in the context of static electromechanics. Its extension to electro-
 elastodynamics is then carried out by defining the appropriate action integral. After derivation of
 the stationary conditions of the action integral, Section 5 introduces a new one-step implicit EM
 time integrator scheme for electro-elastodynamics. Section 6 briefly describes the finite element
 implementation of the new time integrator scheme and Section 7 presents five numerical examples
 in order to validate the conservation properties and robustness of the new scheme. Finally, Section
 8 provides some concluding remarks. Appendix A outlines the definition of the discrete derivative
 expressions featuring in the proposed time integrator in Section 5.

2. Nonlinear continuum electromechanics

A brief introduction into nonlinear continuum electromechanics and the relevant governing
 equations will be presented in this section.

2.1. Kinematics: motion and deformation

Let us consider the motion of an EAP with reference configuration $\mathcal{B}_0 \in \mathbb{R}^3$ and its boundary
 $\partial\mathcal{B}_0$ with unit outward normal \mathbf{N} (refer to Figure 1). After the motion, the EAP occupies a
 deformed configuration $\mathcal{B} \in \mathbb{R}^3$ with boundary $\partial\mathcal{B}$ and unit outward normal \mathbf{n} . The motion of
 the EAP is defined by the deformation mapping $\phi(\mathbf{X}, t)$, which links a material particle from the
 reference configuration $\mathbf{X} \in \mathcal{B}_0$ to the deformed configuration $\mathbf{x} \in \mathcal{B}$ according to $\mathbf{x} = \phi(\mathbf{X}, t)$,
 where displacement boundary conditions can be defined as $\phi(\mathbf{X}, t) = \bar{\phi}(\mathbf{X}, t)$, $\forall \mathbf{X} \in \partial_\phi\mathcal{B}_0$,
 with $\partial_\phi\mathcal{B}_0 \subset \partial\mathcal{B}_0$. Associated with the mapping $\phi(\mathbf{X}, t)$ it is possible to define the two-field
 deformation gradient tensor \mathbf{F} [11, 22, 16, 4] as

$$\mathbf{F} = \nabla_0 \phi(\mathbf{X}, t), \quad (1)$$

where ∇_0 represents the material gradient operator, namely $\nabla_0(\bullet) = \frac{\partial(\bullet)}{\partial\mathbf{X}}$. The deformation
 gradient tensor \mathbf{F} is also referred to as the fibre-map as it relates a fibre of differential length
 from the material configuration $d\mathbf{X}$ to the deformed configuration $d\mathbf{x}$ as $d\mathbf{x} = \mathbf{F}d\mathbf{X}$.

In addition, a differential element area vector in the reference configuration $d\mathbf{A}$ (colinear with
 \mathbf{N}) is mapped to the deformed configuration $d\mathbf{a}$ (colinear with \mathbf{n}) by means of the two-point
 co-factor or adjoint tensor \mathbf{H} as $d\mathbf{a} = \mathbf{H}d\mathbf{A}$. Finally, a differential volume in the reference
 configuration dV is mapped to the final configuration dv via the Jacobian J as $dv = JdV$ (refer
 to Figure 1). Both \mathbf{H} and J can be related to the deformation gradient tensor \mathbf{F} as

$$\mathbf{H} = (\det\mathbf{F}) \mathbf{F}^{-T}; \quad J = \det\mathbf{F}. \quad (2)$$

An equivalent expression to that in equation (2) for both \mathbf{H} and J can be obtained by making
 use of the tensor cross product operation introduced by de Boer [15] and defined as

$$\mathbf{H} = \frac{1}{2} \mathbf{F} \times \mathbf{F}; \quad H_{iI} = \frac{1}{2} \mathcal{E}_{ijk} \mathcal{E}_{IJK} F_{jJ} F_{kK}; \quad (3a)$$

$$J = \frac{1}{3} \mathbf{H} : \mathbf{F}; \quad J = \frac{1}{3} H_{iI} F_{iI}, \quad (3b)$$

where \mathcal{E}_{ijk} (or \mathcal{E}_{IJK}) symbolises the third order alternating tensor components⁴ and the use of
 repeated indices implies summation, unless otherwise stated. As shown in References [10, 9], the
 definitions of \mathbf{H} and J in (3), although equivalent to those in (2), are very appealing as they
 yield simpler expressions for their directional derivatives [9, 10, 20, 37, 36, 19].

⁴Lower case indices $\{i, j, k\}$ will be used to represent the spatial configuration whereas capital case indices
 $\{I, J, K\}$ will be used to represent the material description.

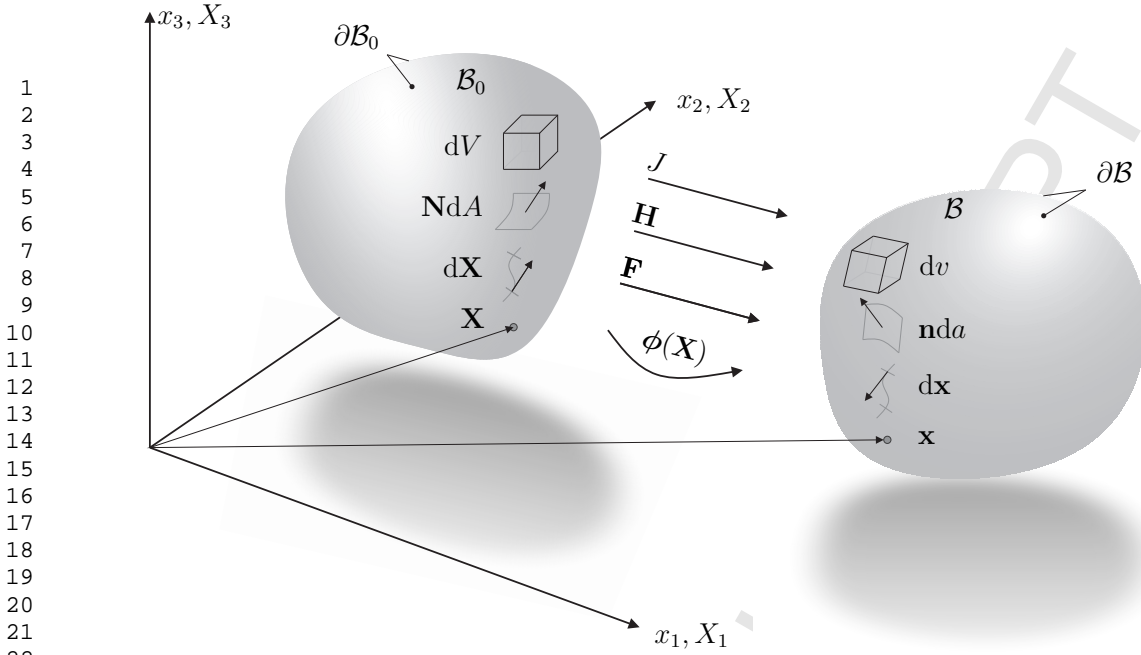


Figure 1: Deformation mapping $\phi(\mathbf{X}, t)$ and main kinematic strain measures $\{\mathbf{F}, \mathbf{H}, J\}$.

2.2. Governing equations in nonlinear electromechanics: conservation of linear momentum and angular momentum

The local form of the conservation of linear momentum [22] can be written as

$$\begin{aligned} \rho_0 \dot{\mathbf{v}} - \text{DIV}(\mathbf{F}\mathbf{S}) - \mathbf{f}_0 &= \mathbf{0}; & \text{in } \mathcal{B}_0; \\ (\mathbf{F}\mathbf{S})\mathbf{N} &= \mathbf{t}_0; & \text{on } \partial_t \mathcal{B}_0; \\ \phi &= \bar{\phi}; & \text{on } \partial_\phi \mathcal{B}_0, \end{aligned} \quad (4)$$

where $\rho_0 : \mathcal{B}_0 \rightarrow \mathbb{R}^+$ represents the mass density of the EAP in the reference configuration, \mathbf{v} the velocity field and $(\dot{\bullet})$ denotes differentiation with respect to time. Furthermore, \mathbf{f}_0 represents a body force per unit undeformed volume \mathcal{B}_0 and \mathbf{t}_0 , the traction force per unit undeformed area applied on $\partial_t \mathcal{B}_0 \subset \partial \mathcal{B}_0$, such that $\partial_t \mathcal{B}_0 \cup \partial_\phi \mathcal{B}_0 = \partial \mathcal{B}_0$ and $\partial_t \mathcal{B}_0 \cap \partial_\phi \mathcal{B}_0 = \emptyset$. Finally, \mathbf{S} represents the second Piola-Kirchhoff stress tensor and the local conservation of angular momentum leads to the well-known tensor condition $\mathbf{S} = \mathbf{S}^T$.

2.3. Governing equations in non-linear electromechanics: Gauss's and Faraday's laws

In the absence of magnetic and time dependant effects, Maxwell equations reduce to Gauss and Faraday laws. The local form of the Gauss law [49, 34, 33] can be written in a Lagrangian setting as

$$\begin{aligned} \text{DIV} \mathbf{D}_0 - \rho_0^e &= 0; & \text{in } \mathcal{B}_0; \\ \mathbf{D}_0 \cdot \mathbf{N} &= -\omega_0^e; & \text{on } \partial_\omega \mathcal{B}_0, \end{aligned} \quad (5)$$

where \mathbf{D}_0 is the Lagrangian electric displacement vector, ρ_0^e represents an electric volume charge per unit of undeformed volume \mathcal{B}_0 and ω_0^e , an electric surface charge per unit of undeformed area $\partial_\omega \mathcal{B}_0 \subset \partial \mathcal{B}_0$. Alternatively, the spatial electric displacement vector \mathbf{D} can be obtained through the area push forward relationship $\mathbf{D}_0 = \mathbf{H}^T \mathbf{D}$, [17, 18]. Furthermore, in the absence of magnetic

fields, the local form of the static Faraday's law can be written in a Lagrangian setting as

$$\begin{aligned} \mathbf{E}_0 &= -\nabla_0\varphi; & \text{in } \mathcal{B}_0; \\ \varphi &= \bar{\varphi}; & \text{on } \partial_\varphi\mathcal{B}_0, \end{aligned} \quad (6)$$

where \mathbf{E}_0 is the Lagrangian electric field vector and φ , the scalar electric potential. In (6), $\partial_\varphi\mathcal{B}_0$ represents the part of the boundary $\partial\mathcal{B}_0$ where essential electric potential boundary conditions are applied such that $\partial_\omega\mathcal{B}_0 \cup \partial_\varphi\mathcal{B}_0 = \partial\mathcal{B}_0$ and $\partial_\omega\mathcal{B}_0 \cap \partial_\varphi\mathcal{B}_0 = \emptyset$. The spatial electric field vector \mathbf{E} can be obtained through the standard fibre transformation $\mathbf{E}_0 = \mathbf{F}^T \mathbf{E}$ [17, 18].

3. Constitutive equations in nonlinear electro-elasticity

The governing equations presented in Section 2 are coupled by means of a suitable constitutive law. The objective of the following section is to introduce some notions on constitutive laws in nonlinear electro-elasticity.

3.1. Multi-variable convexity

In the case of reversible electro-elasticity, the internal energy density e per unit of undeformed volume can be defined in terms of the deformation and the electric displacement field, namely $e = e(\nabla_0\phi, \mathbf{D}_0)$ [34]. Motivated solely by considerations of material stability, Gil and Ortigosa [20, 37, 36, 39] extended the concept of polyconvexity [1, 2, 3] to the context of electromechanics and defined new convexity restrictions on the internal energy, postulating a convex multi-variable definition as

$$e(\nabla_0\phi, \mathbf{D}_0) = W(\mathbf{F}, \mathbf{H}, J, \mathbf{D}_0, \mathbf{d}); \quad \mathbf{d} = \mathbf{F}\mathbf{D}_0, \quad (7)$$

where W must be a convex function with respect to the extended set $\mathcal{V} = \{\mathbf{F}, \mathbf{H}, J, \mathbf{D}_0, \mathbf{d}\}$. Crucially, the above convex multi-variable representation in (7) satisfies the concept of ellipticity for the entire range of deformations and electric displacement fields. In addition, for the requirement of objectivity, the convex multi-variable energy W (7) can be re-expressed in terms of a set of objective arguments as

$$e(\nabla_0\phi, \mathbf{D}_0) = \tilde{e}(\mathbf{C}, \mathbf{D}_0) = \widetilde{W}_{\text{obj}}(\mathbf{C}, \mathbf{G}, C, \mathbf{D}_0, \mathbf{C}\mathbf{D}_0) = \widetilde{W}(\mathbf{C}, \mathbf{G}, C, \mathbf{D}_0), \quad (8)$$

where \tilde{e} represents the internal energy in terms of the right Cauchy-Green strain tensor \mathbf{C} and \mathbf{D}_0 and \widetilde{W} denotes the internal energy expressed in terms of the extended symmetric mechanical kinematic set $\{\mathbf{C}, \mathbf{G}, C\}$, defined as

$$\mathbf{C} = \mathbf{F}^T \mathbf{F}; \quad \mathbf{G} = \frac{1}{2} \mathbf{C} \times \mathbf{C} = \mathbf{H}^T \mathbf{H}; \quad C = \frac{1}{3} \mathbf{G} : \mathbf{C} = J^2, \quad (9)$$

and \mathbf{D}_0 . Notice in equation (8) the argument $\mathbf{C}\mathbf{D}_0$ has been removed from $\widetilde{W}_{\text{obj}}$ as it is redundant (it can be expressed in terms of \mathbf{C} and \mathbf{D}_0). It is worth noting that \widetilde{W} is not convex with respect to the individual components of the set $\tilde{\mathcal{V}} = \{\mathbf{C}, \mathbf{G}, C, \mathbf{D}_0\}$, but rather an objective (frame invariant) re-expression of the convex multi-variable functional W . In this case⁵,

$$D\tilde{e}(\mathbf{C}, \mathbf{D}_0)[\delta\phi] = \mathbf{S} : \frac{1}{2} D\mathbf{C}[\delta\phi]; \quad D\tilde{e}(\mathbf{C}, \mathbf{D}_0)[\delta\mathbf{D}_0] = \mathbf{E}_0 \cdot \delta\mathbf{D}_0, \quad (10)$$

where the second Piola-Kirchhoff stress tensor \mathbf{S} and the material electric field \mathbf{E}_0 are defined in terms of the derivatives of the internal energy $\tilde{e}(\mathbf{C}, \mathbf{D}_0)$, namely

$$\mathbf{S} = 2\partial_{\mathbf{C}}\tilde{e}(\mathbf{C}, \mathbf{D}_0); \quad \mathbf{E}_0 = \partial_{\mathbf{D}_0}\tilde{e}(\mathbf{C}, \mathbf{D}_0). \quad (11)$$

⁵Use of the first law of thermodynamics and consideration of reversibility has been made of.

An alternative but equivalent definition of the directional derivatives of the internal energy $\tilde{e}(\mathbf{C}, \mathbf{D}_0)$ to those in (10) can be obtained by considering its equivalent extended representation \tilde{W} ,

$$D\tilde{W}[\delta\phi] = \partial_{\mathbf{C}}\tilde{W} : DC[\delta\phi] + \partial_{\mathbf{G}}\tilde{W} : DG[\delta\phi] + \partial_{\mathbf{C}}\tilde{W} DC[\delta\phi]; \quad D\tilde{W}[\delta\mathbf{D}_0] = \partial_{\mathbf{D}_0}\tilde{W} \cdot \delta\mathbf{D}_0. \quad (12)$$

From the definition of \mathbf{C} in (9)_a, it is possible to obtain an expression for its directional derivative appearing in equation (12), as

$$DC[\delta\phi] = (\nabla_0\delta\phi)^T \mathbf{F} + \mathbf{F}^T \nabla_0\delta\phi. \quad (13)$$

Similarly, from the definition of \mathbf{G} in (9)_b, its directional derivative can be obtained as

$$DG[\delta\phi] = \mathbf{C} \times DC[\delta\phi]. \quad (14)$$

From equation (9)_c, the directional derivative of C can be obtained as

$$DC[\delta\phi] = \frac{1}{3} (DG[\delta\phi] : \mathbf{C} + \mathbf{G} : DC[\delta\phi]) = \frac{1}{3} (\mathbf{C} \times \mathbf{C} + \mathbf{G}) : DC[\delta\phi] = \mathbf{G} : DC[\delta\phi], \quad (15)$$

Finally, inserting (13), (14) and (15) into (12)_a and comparison with (10)_a enables to obtain an equivalent expression for \mathbf{S} and \mathbf{E}_0 to those in equations (11)_a and (11)_b, respectively, as

$$\mathbf{S} = 2\partial_{\mathbf{C}}\tilde{W} + 2\partial_{\mathbf{G}}\tilde{W} \times \mathbf{C} + 2\partial_{\mathbf{C}}\tilde{W} \mathbf{G}; \quad \mathbf{E}_0 = \partial_{\mathbf{D}_0}\tilde{W}. \quad (16)$$

3.2. Simple examples of convex multi-variable electro-mechanical constitutive models

It is customary to propose an additive decomposition of the internal energy $\tilde{e}(\mathbf{C}, \mathbf{D}_0)$ into a purely mechanical contribution and a coupled electromechanical contribution [12, 54, 27] as

$$\tilde{e}(\mathbf{C}, \mathbf{D}_0) = \tilde{e}_m(\mathbf{C}) + \tilde{e}_{em}(\mathbf{C}, \mathbf{D}_0). \quad (17)$$

The simplest expression for the electromechanical contribution corresponds to that of an ideal dielectric elastomer, defined as

$$\tilde{e}_{em}(\mathbf{C}, \mathbf{D}_0) = \tilde{W}_{em}(\mathbf{C}, \mathbf{C}, \mathbf{D}_0) = \frac{1}{2\varepsilon_r\varepsilon_0 C^{1/2}} \mathbf{D}_0 \cdot \mathbf{C} \mathbf{D}_0, \quad (18)$$

where ε_0 represents the permittivity of vacuum, with $\varepsilon_0 = 8.8541 \times 10^{-12} \text{NC}^{-2}\text{m}^{-2}$. Different models can be proposed for the purely mechanical contribution \tilde{e}_m . The Mooney-Rivlin model is defined via the following polyconvex energy functional

$$\tilde{e}_m^{MR}(\mathbf{C}) = \tilde{W}_m^{MR}(\mathbf{C}, \mathbf{G}, C) = \frac{\mu_1}{2} \text{tr} \mathbf{C} + \frac{\mu_2}{2} \text{tr} \mathbf{G} - (\mu_1 + 2\mu_2) \ln C^{1/2} - \frac{\lambda}{2} (C^{1/2} - 1)^2, \quad (19)$$

where μ_1 , μ_2 and λ are material parameters with units of stress related to the shear modulus μ_0 and the bulk modulus λ_0 in the origin as $\mu_0 = \mu_1 + \mu_2$ and $\lambda_0 = \lambda + 2\mu_2$. The Gent model, based on the concept of limiting chain extensibility, has also been frequently used to define the purely mechanical contribution of dielectric elastomers. The internal energy for this model is defined as

$$\tilde{e}_m^G(\mathbf{C}) = \tilde{W}_m^G(\mathbf{C}, C) = -\frac{\mu(I_{\max} - 3)}{2} \ln \left(1 - \frac{\text{tr} \mathbf{C} - 3}{I_{\max} - 3} \right) - \mu \ln C^{1/2} + \frac{\kappa}{2} (C^{1/2} - 1)^2, \quad (20)$$

with $\mu_0 = \mu$ and $\lambda_0 = \lambda + 2\mu/(I_{\max} - 3)$. In addition, I_{\max} represents the limiting value of the first invariant of \mathbf{C} , namely $\text{tr} \mathbf{C}$. Notice that \tilde{e}_m^G in (20) is polyconvex for the range $\text{tr} \mathbf{C} < I_{\max}$. Hence, for a convex multi-variable electromechanical contribution \tilde{e}_{em} , then the addition of both \tilde{e}_m^G and \tilde{e}_{em} is also convex multi-variable for that range.

3.3. The Helmholtz energy function

The convex multi-variable nature of the internal energy $e(\nabla_0\phi, \mathbf{D}_0)$ ensures convexity of $e(\nabla_0\phi, \mathbf{D}_0)$, $\tilde{e}(\mathbf{C}, \mathbf{D}_0)$ and $\tilde{W}(\mathbf{C}, \mathbf{G}, C, \mathbf{D}_0)$ with respect to \mathbf{D}_0 . Consequently, a one-to-one and invertible relationship between variables \mathbf{D}_0 and \mathbf{E}_0 can always be established. Therefore, it is possible to make use of a partial Legendre transform of the internal energy which leads to the definition of the Helmholtz energy functional $\tilde{W}_\phi(\mathbf{C}, \mathbf{G}, C, \mathbf{E}_0)$ as

$$\tilde{W}_\phi(\mathbf{C}, \mathbf{G}, C, \mathbf{E}_0) = -\sup_{\mathbf{D}_0} \left\{ \mathbf{E}_0 \cdot \mathbf{D}_0 - \tilde{W}(\mathbf{C}, \mathbf{G}, C, \mathbf{D}_0) \right\}, \quad (21)$$

where use of (16)_b has been made of.

Remark 1. From the additive decomposition in equation (17), the Helmholtz energy functional $\tilde{W}_\phi(\mathbf{C}, \mathbf{G}, C, \mathbf{E}_0)$ can be also additively decomposed as

$$\tilde{W}_\phi(\mathbf{C}, \mathbf{G}, C, \mathbf{E}_0) = \tilde{W}_{\phi_m}(\mathbf{C}, \mathbf{G}, C) + \tilde{W}_{\phi_{em}}(\mathbf{C}, \mathbf{G}, C, \mathbf{E}_0), \quad (22)$$

where the mechanical component \tilde{W}_{ϕ_m} is exactly identical to that of \tilde{W} , namely

$$\tilde{W}_{\phi_m}(\mathbf{C}, \mathbf{G}, C) = \tilde{W}_m(\mathbf{C}, \mathbf{G}, C). \quad (23)$$

When the electromechanical contribution is that of an ideal dielectric elastomer as that in (18), it is possible to obtain an explicit representation of $\tilde{W}_{\phi_{em}}$ by making use of (21) as

$$\tilde{W}_{\phi_{em}}(\mathbf{G}, C, \mathbf{E}_0) = -\frac{\varepsilon_r \varepsilon_0}{2C^{1/2}} \mathbf{E}_0 \cdot \mathbf{G} \mathbf{E}_0. \quad (24)$$

However, for a more complex energy functional than that of an ideal dielectric elastomer, it is generally impossible to obtain an explicit representation for the Helmholtz functional $\tilde{W}_{\phi_{em}}(\mathbf{C}, \mathbf{G}, C, \mathbf{E}_0)$ associated with $\tilde{W}_{em}(\mathbf{C}, \mathbf{G}, C, \mathbf{D}_0)$. A simple example for the internal energy functional that showcases this difficulty is

$$\tilde{W}_{em}(\mathbf{C}, C, \mathbf{D}_0) = \frac{1}{2\varepsilon_1 C^{1/2}} \mathbf{D}_0 \cdot \mathbf{C} \mathbf{D}_0 + \frac{1}{2\alpha C^{1/2}} (\mathbf{D}_0 \cdot \mathbf{C} \mathbf{D}_0)^p; \quad p \geq 2, \quad (25)$$

with ε_1 an electric permittivity-like material parameter (units of N/m^2) and α , a material parameter with units of $V^4/(Nm^2)$.

4. Electro-Elastodynamics

The objective of this section is to present the variational formulation that will be used in order to develop an EM time integration scheme in Section 5.

4.1. Point of departure: three-field mixed formulation for electro-mechanics

A three-field mixed variational principle in the context of static electro-mechanics (where inertial effects are not considered) can be defined as

$$\Pi_{\tilde{W}}(\phi, \varphi, \mathbf{D}_0) = \inf_{\phi, \mathbf{D}_0} \sup_{\varphi} \left\{ \int_{\mathcal{B}_0} \tilde{W}(\mathbf{C}, \mathbf{G}, C, \mathbf{D}_0) dV + \int_{\mathcal{B}_0} \mathbf{D}_0 \cdot \nabla_0 \varphi dV - \Pi_{\text{ext}}^m(\phi) - \Pi_{\text{ext}}^e(\varphi) \right\}. \quad (26)$$

The reader is referred to Reference [20] for the derivation of above variational principle. In (26), the external contributions Π_{ext}^m and Π_{ext}^e are defined as

$$\Pi_{\text{ext}}^m(\boldsymbol{\phi}) = \int_{\mathcal{B}_0} \mathbf{f}_0 \cdot \boldsymbol{\phi} dV + \int_{\partial_t \mathcal{B}_0} \mathbf{t}_0 \cdot \boldsymbol{\phi} dA; \quad \Pi_{\text{ext}}^e(\varphi) = - \int_{\mathcal{B}_0} \rho_0^e \varphi dV - \int_{\partial_\omega \mathcal{B}_0} \omega_0^e \varphi dA. \quad (27)$$

In equation (26), $\{\boldsymbol{\phi}, \varphi, \mathbf{D}_0\} \in \mathbb{V}^\phi \times \mathbb{V}^\varphi \times \mathbb{V}^{\mathbf{D}_0}$, as

$$\begin{aligned} \mathbb{V}^\phi &= \{\boldsymbol{\phi} : \mathcal{B}_0 \rightarrow \mathbb{R}^3; \quad (\boldsymbol{\phi})_i \in H^1(\mathcal{B}_0) \mid J > 0\}; \\ \mathbb{V}^\varphi &= \{\varphi : \mathcal{B}_0 \rightarrow \mathbb{R}^1; \quad \varphi \in H^1(\mathcal{B}_0)\}; \\ \mathbb{V}^{\mathbf{D}_0} &= \{\mathbf{D}_0 : \mathcal{B}_0 \rightarrow \mathbb{R}^3; \quad (\mathbf{D}_0)_I \in L_2(\mathcal{B}_0)\}, \end{aligned} \quad (28)$$

Similarly, let us consider admissible variations $\{\delta\boldsymbol{\phi}, \delta\varphi, \delta\mathbf{D}_0\} \in \mathbb{V}_0^\phi \times \mathbb{V}_0^\varphi \times \mathbb{V}^{\mathbf{D}_0}$, with

$$\begin{aligned} \mathbb{V}_0^\phi &= \{\forall \boldsymbol{\phi} \in \mathbb{V}^\phi; \quad \boldsymbol{\phi} = \mathbf{0} \text{ on } \partial_\phi \mathcal{B}_0\}; \\ \mathbb{V}_0^\varphi &= \{\forall \varphi \in \mathbb{V}^\varphi; \quad \varphi = 0 \text{ on } \partial_\varphi \mathcal{B}_0\}. \end{aligned} \quad (29)$$

The stationary conditions of the mixed variational principle $\Pi_{\widetilde{W}}$ in (26) yield

$$\begin{aligned} D\Pi_{\widetilde{W}}[\delta\boldsymbol{\phi}] &= \int_{\mathcal{B}_0} \mathbf{S} : \frac{1}{2} D\mathbf{C}[\delta\boldsymbol{\phi}] dV - \int_{\mathcal{B}_0} \mathbf{f}_0 \cdot \delta\boldsymbol{\phi} dV - \int_{\partial_t \mathcal{B}_0} \mathbf{t}_0 \cdot \delta\boldsymbol{\phi} dA = 0; \\ D\Pi_{\widetilde{W}}[\delta\varphi] &= \int_{\mathcal{B}_0} \mathbf{D}_0 \cdot \nabla_0 \delta\varphi dV + \int_{\mathcal{B}_0} \rho_0^e \delta\varphi dV + \int_{\partial_\omega \mathcal{B}_0} \omega_0^e \delta\varphi dA = 0; \\ D\Pi_{\widetilde{W}}[\delta\mathbf{D}_0] &= \int_{\mathcal{B}_0} \delta\mathbf{D}_0 \cdot (\partial_{\mathbf{D}_0} \widetilde{W} + \nabla_0 \varphi) dV = 0, \end{aligned} \quad (30)$$

with \mathbf{S} defined in (16)_a. Above equation (30)_a represents the weak form of the local balance of linear momentum in (4) for the case where no inertia effects are considered. In addition, equation (30)_b corresponds to the weak form of the Gauss law in (5). Finally, equation (30)_c represents the weak form of the Faraday law in (6).

Remark 2. Starting from the total potential $\Pi_{\widetilde{W}}$ in (26), use of the Legendre transformation in (21) leads to a two-field formulation with unknowns $\{\boldsymbol{\phi}, \varphi\}$ in terms of the Helmholtz functional (refer to Remark 1) as

$$\Pi_{\widetilde{W}_\phi}(\boldsymbol{\phi}, \varphi) = \inf_{\boldsymbol{\phi}} \sup_{\varphi} \left\{ \int_{\mathcal{B}_0} \widetilde{W}_\phi(\mathbf{C}, \mathbf{G}, C, \mathbf{E}_0) dV - \Pi_{\text{ext}}^m(\boldsymbol{\phi}) - \Pi_{\text{ext}}^e(\varphi) \right\}. \quad (31)$$

The stationary conditions of the above variational principle are

$$\begin{aligned} D\Pi_{\widetilde{W}_\phi}[\delta\boldsymbol{\phi}] &= \int_{\mathcal{B}_0} \mathbf{S} : \frac{1}{2} D\mathbf{C}[\delta\boldsymbol{\phi}] dV - \int_{\mathcal{B}_0} \mathbf{f}_0 \cdot \delta\boldsymbol{\phi} dV - \int_{\partial_t \mathcal{B}_0} \mathbf{t}_0 \cdot \delta\boldsymbol{\phi} dA = 0; \\ D\Pi_{\widetilde{W}_\phi}[\delta\varphi] &= - \int_{\mathcal{B}_0} \partial_{\mathbf{E}_0} \widetilde{W}_\phi \cdot \nabla_0 \delta\varphi dV + \int_{\mathcal{B}_0} \rho_0^e \delta\varphi dV + \int_{\partial_\omega \mathcal{B}_0} \omega_0^e \delta\varphi dA = 0, \end{aligned} \quad (32)$$

with

$$\mathbf{S} = 2\partial_{\mathbf{C}} \widetilde{W}_\phi + 2\partial_{\mathbf{G}} \widetilde{W}_\phi \times \mathbf{C} + 2\partial_C \widetilde{W}_\phi \mathbf{G}. \quad (33)$$

The variational principle in (31) is typically preferred in finite element implementations. However, the a priori definition of a materially stable Helmholtz functional is not in general possible due to its saddle point nature. Therefore, we advocate in this paper for the definition of materially stable convex multi-variable internal energy functionals $\widetilde{W}(\mathbf{C}, \mathbf{G}, C, \mathbf{D}_0)$ (featuring in the three-field principle $\Pi_{\widetilde{W}}$) which through (21), yield materially stable Helmholtz energy functionals [20].

4.2. Extension to electro-elastodynamics

The objective of this section is to generalise the mixed variational principle $\Pi_{\widetilde{W}}$ in (26) to the context of electro-elastodynamics. This can be done by considering the following action integral

$$L_{\widetilde{W}}(\mathbf{v}, \boldsymbol{\phi}, \varphi, \mathbf{D}_0) = \int_{t_0}^t \left(\int_{\mathcal{B}_0} \left(\dot{\boldsymbol{\phi}} - \frac{1}{2} \mathbf{v} \right) \cdot \rho_0 \mathbf{v} dV - \int_{\mathcal{B}_0} \widetilde{W}(\mathbf{C}, \mathbf{G}, C, \mathbf{D}_0) dV - \int_{\mathcal{B}_0} \mathbf{D}_0 \cdot \nabla_0 \varphi dV + \Pi_{\text{ext}}^m(\boldsymbol{\phi}) + \Pi_{\text{ext}}^e(\varphi) \right) dt, \quad (34)$$

where t_0 and t represent any two instances of time with $t > t_0$. By means of Hamilton's principle, the stationary conditions of the action integral $L_{\widetilde{W}}$ in (34) are

$$\begin{aligned} \mathcal{W}_{\mathbf{v}} &= \int_{\mathcal{B}_0} (\mathbf{v} - \dot{\boldsymbol{\phi}}) \cdot \rho_0 \delta \mathbf{v} dV = 0; \\ \mathcal{W}_{\boldsymbol{\phi}} &= \int_{\mathcal{B}_0} \rho_0 \dot{\mathbf{v}} \cdot \delta \boldsymbol{\phi} dV + \int_{\mathcal{B}_0} \mathbf{S} : \frac{1}{2} D\mathbf{C}[\delta \boldsymbol{\phi}] dV - \int_{\mathcal{B}_0} \mathbf{f}_0 \cdot \delta \boldsymbol{\phi} dV - \int_{\partial_t \mathcal{B}_0} \mathbf{t}_0 \cdot \delta \boldsymbol{\phi} dA = 0; \\ \mathcal{W}_{\varphi} &= \int_{\mathcal{B}_0} \mathbf{D}_0 \cdot \nabla_0 \delta \varphi dV + \int_{\mathcal{B}_0} \rho_0^e \delta \varphi dV + \int_{\partial_{\omega} \mathcal{B}_0} \omega_0^e \delta \varphi dA = 0; \\ \mathcal{W}_{\mathbf{D}_0} &= \int_{\mathcal{B}_0} \delta \mathbf{D}_0 \cdot (\partial_{\mathbf{D}_0} \widetilde{W} + \nabla_0 \varphi) dV = 0, \end{aligned} \quad (35)$$

and with $\{\mathbf{v}, \boldsymbol{\phi}, \varphi, \mathbf{D}_0\} \in \mathbb{V}^{\boldsymbol{\phi}} \times \mathbb{V}^{\boldsymbol{\phi}} \times \mathbb{V}^{\varphi} \times \mathbb{V}^{\mathbf{D}_0}$ and $\{\delta \mathbf{v}, \delta \boldsymbol{\phi}, \delta \varphi, \delta \mathbf{D}_0\} \in \mathbb{V}_0^{\boldsymbol{\phi}} \times \mathbb{V}_0^{\boldsymbol{\phi}} \times \mathbb{V}_0^{\varphi} \times \mathbb{V}_0^{\mathbf{D}_0}$. Note that an integration by parts with respect to time has been used on the first term on the right hand-side of (35)_b. Equation (35)_a represents the weak form for the relationship between the velocity field \mathbf{v} and the time derivative of the mapping $\boldsymbol{\phi}$ and equation (35)_b, the extension of the weak form of the balance of linear momentum in (30)_a to electro-elastodynamics (hence the equation is supplemented with the inertia term). Finally, notice that both weak forms for the Gauss and Faraday laws in (35)_c and (35)_d are identical to those in the static case in (30)_b and (30)_c, respectively.

Remark 3. When pursuing a Helmholtz-based mixed formulation (see Remark 2), the following action integral can be defined in order to extend the variational principle $\Pi_{\widetilde{W}_{\boldsymbol{\phi}}}$ to the case of electro-elastodynamics,

$$L_{\widetilde{W}_{\boldsymbol{\phi}}}(\mathbf{v}, \boldsymbol{\phi}, \varphi) = \int_{t_0}^t \left(\int_{\mathcal{B}_0} \left(\dot{\boldsymbol{\phi}} - \frac{1}{2} \mathbf{v} \right) \cdot \rho_0 \mathbf{v} dV - \int_{\mathcal{B}_0} \widetilde{W}_{\boldsymbol{\phi}}(\mathbf{C}, \mathbf{G}, C, \mathbf{E}_0) dV + \Pi_{\text{ext}}^m(\boldsymbol{\phi}) + \Pi_{\text{ext}}^e(\varphi) \right) dt. \quad (36)$$

The stationary conditions of the above action integral (36) are

$$\begin{aligned} \mathcal{W}_{\mathbf{v}} &= \int_{\mathcal{B}_0} (\mathbf{v} - \dot{\boldsymbol{\phi}}) \cdot \rho_0 \delta \mathbf{v} dV = 0; \\ \mathcal{W}_{\boldsymbol{\phi}} &= \int_{\mathcal{B}_0} \rho_0 \dot{\mathbf{v}} \cdot \delta \boldsymbol{\phi} dV + \int_{\mathcal{B}_0} \mathbf{S} : \frac{1}{2} D\mathbf{C}[\delta \boldsymbol{\phi}] dV - \int_{\mathcal{B}_0} \mathbf{f}_0 \cdot \delta \boldsymbol{\phi} dV - \int_{\partial_t \mathcal{B}_0} \mathbf{t}_0 \cdot \delta \boldsymbol{\phi} dA = 0; \\ \mathcal{W}_{\varphi} &= - \int_{\mathcal{B}_0} \partial_{\mathbf{E}_0} \widetilde{W}_{\boldsymbol{\phi}} \cdot \nabla_0 \delta \varphi dV + \int_{\mathcal{B}_0} \rho_0^e \delta \varphi dV + \int_{\partial_{\omega} \mathcal{B}_0} \omega_0^e \delta \varphi dA = 0, \end{aligned} \quad (37)$$

with \mathbf{S} defined in (33) and integration by parts with respect to time has been applied on the second term on the right hand side of (37)_b.

4.3. Balance laws and integrals in electro-elastodynamics

Starting with the stationary conditions (35) the following sections derive the global conservation laws that govern the motion of the EAP.

4.3.1. Global form for conservation of linear momentum

For a displacement field $\delta\phi = \xi$, with $\mathbb{R}^3 \ni \xi = \text{const.}$, the stationary condition in (35)_b leads to the global form of the conservation of linear momentum, namely

$$\dot{\mathbf{L}} - \mathbf{F}^{\text{ext}} = \mathbf{0}; \quad \mathbf{L} = \int_{\mathcal{B}_0} \rho_0 \mathbf{v} dV; \quad \mathbf{F}^{\text{ext}} = \int_{\partial_t \mathcal{B}_0} \mathbf{t}_0 dA + \int_{\mathcal{B}_0} \mathbf{f}_0 dV, \quad (38)$$

where \mathbf{L} represents the total linear momentum and \mathbf{F}^{ext} , the total external force. From (38) it is possible to conclude that \mathbf{L} is a constant of motion for the case of vanishing external forces \mathbf{F}^{ext} .

4.3.2. Global form for conservation of angular momentum

For a rotational field $\delta\phi = \xi \times \phi$, with $\mathbb{R}^3 \ni \xi = \text{const.}$, the stationary condition in (35)_b leads to the global form of the conservation of angular momentum, namely

$$\dot{\mathbf{J}} - \mathbf{M}^{\text{ext}} = \mathbf{0}; \quad \mathbf{J} = \int_{\mathcal{B}_0} \phi \times \rho_0 \mathbf{v} dV; \quad \mathbf{M}^{\text{ext}} = \int_{\partial_t \mathcal{B}_0} \phi \times \mathbf{t}_0 dA + \int_{\mathcal{B}_0} \phi \times \mathbf{f}_0 dV, \quad (39)$$

where \mathbf{J} represents the total angular momentum and \mathbf{M}^{ext} , the total external torque. From (39), it is clear that \mathbf{J} is a constant of motion for vanishing external torques \mathbf{M}^{ext} .

4.3.3. Global form for Gauss' law

Taking $\delta\varphi = \xi$, with $\mathbb{R} \ni \xi = \text{const.}$, the stationary condition \mathcal{W}_φ in (35)_c leads to the global form of the Gauss' law

$$\int_{\mathcal{B}_0} \rho_0^e dV + \int_{\partial_\omega \mathcal{B}_0} \omega_0^e dA = 0. \quad (40)$$

Then, for time independent volumetric and surface electrical charges ρ_0^e and ω_0^e , equation (40) dictates that the total electric charge of the system is conserved and equal to zero.

4.3.4. Global form for conservation of energy

Let us replace the test functions $\{\delta\mathbf{v}, \delta\phi, \delta\varphi, \delta\mathbf{D}_0\}$ in (35) with $\{\dot{\mathbf{v}}, \dot{\phi}, \dot{\varphi}, \dot{\mathbf{D}}_0\} \in \mathbb{V}_0^\phi \times \mathbb{V}_0^\phi \times \mathbb{V}_0^\varphi \times \mathbb{V}^{\mathbf{D}_0}$. This yields

$$\begin{aligned} \int_{\mathcal{B}_0} (\mathbf{v} - \dot{\phi}) \cdot \rho_0 \dot{\mathbf{v}} dV &= 0; \\ \int_{\mathcal{B}_0} \rho_0 \dot{\mathbf{v}} \cdot \dot{\phi} dV + \int_{\mathcal{B}_0} \mathbf{S} : \frac{1}{2} \dot{\mathbf{C}} dV - \int_{\mathcal{B}_0} \mathbf{f}_0 \cdot \dot{\phi} dV - \int_{\partial_t \mathcal{B}_0} \mathbf{t}_0 \cdot \dot{\phi} dA &= 0; \\ \int_{\mathcal{B}_0} \mathbf{D}_0 \cdot \nabla_0 \dot{\varphi} dV + \int_{\mathcal{B}_0} \rho_0^e \dot{\varphi} dV + \int_{\partial_\omega \mathcal{B}_0} \omega_0^e \dot{\varphi} dA &= 0; \\ \int_{\mathcal{B}_0} \dot{\mathbf{D}}_0 \cdot (\partial_{\mathbf{D}_0} \widetilde{W} + \nabla_0 \varphi) dV &= 0. \end{aligned} \quad (41)$$

Addition of the four equations in (41) leads, in the case of time independent forces \mathbf{f}_0 and \mathbf{t}_0 and charges ρ_0^e and ω_0^e to

$$\dot{K} + \int_{\mathcal{B}_0} \left(\mathbf{S} : \frac{1}{2} \dot{\mathbf{C}} + \partial_{\mathbf{D}_0} \widetilde{W} \cdot \dot{\mathbf{D}}_0 \right) dV + \int_{\mathcal{B}_0} \left(\mathbf{D}_0 \cdot \nabla_0 \dot{\varphi} + \dot{\mathbf{D}}_0 \cdot \nabla_0 \varphi \right) dV - \dot{\Pi}_{\text{ext}}^m(\phi) - \dot{\Pi}_{\text{ext}}^e(\varphi) = 0, \quad (42)$$

where $K = \int_{\mathcal{B}_0} \frac{1}{2} \rho_0 \mathbf{v} \cdot \mathbf{v} dV$ in (42) represents the total kinetic energy of the system. Finally, equation (42) can be re-written as

$$\dot{K} + \int_{\mathcal{B}_0} \dot{\widetilde{W}}(\mathbf{C}, \mathbf{G}, C, \mathbf{D}_0) dV + \int_{\mathcal{B}_0} \frac{d}{dt} (\mathbf{D}_0 \cdot \nabla_0 \varphi) dV - \dot{\Pi}_{\text{ext}}^m(\phi) - \dot{\Pi}_{\text{ext}}^e(\varphi) = 0. \quad (43)$$

It is therefore clear that in the case of time independent forces and electric charges, the following condition holds

$$\dot{\mathcal{H}}_{\widetilde{W}} = 0; \quad \mathcal{H}_{\widetilde{W}} = K + \int_{\mathcal{B}_0} \widetilde{W}(\mathbf{C}, \mathbf{G}, C, \mathbf{D}_0) dV + \int_{\mathcal{B}_0} \mathbf{D}_0 \cdot \nabla_0 \varphi dV - \Pi_{\text{ext}}^m(\phi) - \Pi_{\text{ext}}^e(\varphi), \quad (44)$$

and therefore the scalar field $\mathcal{H}_{\widetilde{W}}$ is preserved throughout the motion of the EAP. Note that $\mathcal{H}_{\widetilde{W}}$ is the total Hamiltonian, defined through the following Legendre transformation

$$\mathcal{H}_{\widetilde{W}}(\mathbf{p}, \phi, \varphi, \mathbf{D}_0) = \sup_{\mathbf{v}} \left\{ \int_{\mathcal{B}_0} \mathbf{p} \cdot \mathbf{v} dV - L_{\widetilde{W}}(\mathbf{v}, \phi, \varphi, \mathbf{D}_0) \right\}, \quad (45)$$

where $\mathbf{p} = \rho_0 \mathbf{v}$ denotes the linear momentum per unit undeformed volume \mathcal{B}_0 .

Remark 4. Identical results to those in Sections 4.3.1, 4.3.2 and 4.3.3 can be obtained for the stationary conditions in (37) of the Helmholtz-based action integral $L_{\widetilde{W}_\phi}$ (36) regarding conservation of linear momentum, angular momentum, and the Gauss law, respectively. For the energy conservation, a similar result to that in equation (44) is obtained as

$$\dot{\mathcal{H}}_{\widetilde{W}_\phi} = 0; \quad \mathcal{H}_{\widetilde{W}_\phi} = K + \int_{\mathcal{B}_0} \widetilde{W}_\phi(\mathbf{C}, \mathbf{G}, C, \mathbf{E}_0) dV - \Pi_{\text{ext}}^m(\phi) - \Pi_{\text{ext}}^e(\varphi), \quad (46)$$

where $\mathcal{H}_{\widetilde{W}_\phi}$ is the counterpart of $\mathcal{H}_{\widetilde{W}}$ for the case of the Helmholtz-based formulation.

5. Energy-Momentum integration scheme for electro-elastodynamics

Following the work of Simo [48], Gonzalez [21], Romero [44] and Betsch et. al. [8, 7] in the context of nonlinear elasticity and Franke et al. [19] in the context of thermoelasticity, the objective of this section is to propose an EM preserving time discretisation scheme for the set of weak forms in (35).

5.1. Design of the EM scheme

Let us consider a sequence of time steps $\{t_1, t_2, \dots, t_n, t_{n+1}\}$, where t_{n+1} denotes the current time step. From the stationary conditions in (35), the following implicit one-step time integrator is proposed

$$\begin{aligned} (\mathcal{W}_{\mathbf{v}})_{\text{algo}} &= \int_{\mathcal{B}_0} \left(\mathbf{v}_{n+1/2} - \frac{\Delta \phi}{\Delta t} \right) \cdot \rho_0 \delta \mathbf{v} dV = 0; \\ (\mathcal{W}_\phi)_{\text{algo}} &= \int_{\mathcal{B}_0} \rho_0 \frac{\Delta \mathbf{v}}{\Delta t} \cdot \delta \phi dV + \int_{\mathcal{B}_0} \mathbf{S}_{\text{algo}} : \frac{1}{2} (D\mathbf{C}[\delta \phi])_{\text{algo}} dV - \int_{\mathcal{B}_0} \mathbf{f}_{0_{n+1/2}} \cdot \delta \phi dV \\ &\quad - \int_{\partial_t \mathcal{B}_0} \mathbf{t}_{0_{n+1/2}} \cdot \delta \phi dA = 0; \\ (\mathcal{W}_\varphi)_{\text{algo}} &= \int_{\mathcal{B}_0} \mathbf{D}_{0_{n+1/2}} \cdot \nabla_0 \delta \varphi dV + \int_{\mathcal{B}_0} \rho_{0_{n+1/2}}^e \delta \varphi dV + \int_{\partial_\omega \mathcal{B}_0} \omega_{0_{n+1/2}}^e \delta \varphi dA = 0; \\ (\mathcal{W}_{\mathbf{D}_0})_{\text{algo}} &= \int_{\mathcal{B}_0} \delta \mathbf{D}_0 \cdot \left(D_{\mathbf{D}_0} \widetilde{W} + \nabla_0 \varphi_{n+1/2} \right) dV = 0. \end{aligned} \quad (47)$$

Note that $(\mathcal{W}_v)_{\text{algo}}$, $(\mathcal{W}_\phi)_{\text{algo}}$, $(\mathcal{W}_\varphi)_{\text{algo}}$ and $(\mathcal{W}_{D_0})_{\text{algo}}$ in (47) represent the algorithmic or time discrete versions of the stationary conditions in (35) and $(\bullet)_{n+1/2} = \frac{1}{2}((\bullet)_{n+1} + (\bullet)_n)$ and $\Delta(\bullet) = (\bullet)_{n+1} - (\bullet)_n$. Noticing the equivalence between (10)_a and (12)_a, the second term on the right-hand side of (47)_b can be expressed as

$$\mathbf{S}_{\text{algo}} : \frac{1}{2} (DC[\delta\phi])_{\text{algo}} = D_C \widetilde{W} : (DC[\delta\phi])_{\text{algo}} + D_G \widetilde{W} : (DG[\delta\phi])_{\text{algo}} + D_C \widetilde{W} (DC[\delta\phi])_{\text{algo}}. \quad (48)$$

In (47) and (48), $\{D_C \widetilde{W}, D_G \widetilde{W}, D_C \widetilde{W}, D_{D_0} \widetilde{W}\}$ represent the discrete derivatives [21, 19] of the internal energy \widetilde{W} with respect to $\{\mathbf{C}, \mathbf{G}, C, \mathbf{D}_0\}$, respectively, which are the algorithmic or time discrete counterparts of $\{\partial_C \widetilde{W}, \partial_G \widetilde{W}, \partial_C \widetilde{W}, \partial_{D_0} \widetilde{W}\}$, respectively. In addition, $(DC[\delta\phi])_{\text{algo}}$, $(DG[\delta\phi])_{\text{algo}}$ and $(DC[\delta\phi])_{\text{algo}}$ represent the algorithmic counterparts of $\{DC[\delta\phi], DG[\delta\phi], DC[\delta\phi]\}$ in (13)-(15).

5.1.1. Discretive derivatives of the internal energy

In this work, we use a definition of the (multiple) discrete derivative expressions $D_C \widetilde{W}$, $D_G \widetilde{W}$, $D_C \widetilde{W}$ and $D_{D_0} \widetilde{W}$ of the internal energy based on the derivation presented in [19] for energies depending upon several arguments. The generic expression for the discrete derivatives $\{D_C \widetilde{W}, D_G \widetilde{W}, D_C \widetilde{W}, D_{D_0} \widetilde{W}\}$ is derived in Appendix A. The expressions given in the Appendix satisfy two crucial properties for the design of EM time integrators, namely:

- They fulfil the so called *directionality property* [19, 21],

$$D_C \widetilde{W} : \Delta \mathbf{C} + D_G \widetilde{W} : \Delta \mathbf{G} + D_C \widetilde{W} \Delta C + D_{D_0} \widetilde{W} \cdot \Delta \mathbf{D}_0 = \Delta \widetilde{W}. \quad (49)$$

- They are well defined in the limit as $\|\Delta \mathbf{C}\| \rightarrow 0$, $\|\Delta \mathbf{G}\| \rightarrow 0$, $\|\Delta C\| \rightarrow 0$ and $\|\Delta \mathbf{D}_0\| \rightarrow 0$.

The first property is critical for the algorithm in (47) to preserve energy under zero or time invariant external forces and electric charges. The second condition ensures that for sufficiently regular solutions

$$\mathbf{S}_{\text{algo}} = \mathbf{S}(\widetilde{V}_{n+1/2}) + O(\Delta t^2); \quad D_{D_0} \widetilde{W} = \partial_{D_0} \widetilde{W}(\widetilde{V}_{n+1/2}) + O(\Delta t^2), \quad (50)$$

and therefore, the proposed EM time integrator is second order accurate.

Remark 5. The consideration of convex multi-variable internal energy functionals ensures the satisfaction of ellipticity at the continuum level. This condition cannot be verified at the (time) discrete level, where the derivatives of the energy are replaced by their discrete counterparts. Ellipticity can only be mathematically proven in the limit, i.e. $\Delta t \rightarrow 0$, when both the discrete and continuum levels coincide (see (50)).

5.1.2. Algorithmic directional derivatives

The objective of this section is to propose appropriate algorithmic expressions for $(DC[\delta\phi])_{\text{algo}}$, $(DG[\delta\phi])_{\text{algo}}$ and $(DC[\delta\phi])_{\text{algo}}$ in (48). In doing so, the following properties will be fulfilled:

- For $\delta\phi = \Delta\phi = \phi_{n+1} - \phi_n$, a desired property to be satisfied is

$$\begin{aligned} D_C \widetilde{W} : (DC[\Delta\phi])_{\text{algo}} &= D_C \widetilde{W} : \Delta \mathbf{C}; \\ D_G \widetilde{W} : (DG[\Delta\phi])_{\text{algo}} &= D_G \widetilde{W} : \Delta \mathbf{G}; \\ D_C \widetilde{W} (DC[\Delta\phi])_{\text{algo}} &= D_C \widetilde{W} \Delta C. \end{aligned} \quad (51)$$

It is easy to verify that the following definition for $(DC[\delta\phi])_{\text{algo}}$, $(DG[\delta\phi])_{\text{algo}}$ and $(DC[\delta\phi])_{\text{algo}}$ (proposed in [19])

$$\begin{aligned} (DC[\delta\phi])_{\text{algo}} &= \left((\nabla_0 \delta\phi)^T \mathbf{F}_{n+1/2} + \mathbf{F}_{n+1/2}^T \nabla_0 \delta\phi \right); \\ (DG[\delta\phi])_{\text{algo}} &= \mathbf{C}_{\text{algo}} \times (DC[\delta\phi])_{\text{algo}}; & \mathbf{C}_{\text{algo}} &= \mathbf{C}_{n+1/2}; \\ (DC[\delta\phi])_{\text{algo}} &= \mathbf{G}_{\text{algo}} : (DC[\delta\phi])_{\text{algo}}; & \mathbf{G}_{\text{algo}} &= \frac{1}{3} (\mathbf{C}_{n+1/2} \times \mathbf{C}_{n+1/2} + \mathbf{G}_{n+1/2}), \end{aligned} \quad (52)$$

satisfies above properties in (51). From equation (48) and making use of (52), the algorithmic second Piola-Kirchhoff stress tensor \mathbf{S}_{algo} in (47) can be defined as

$$\mathbf{S}_{\text{algo}} = 2D_C \widetilde{W} + 2D_G \widetilde{W} \times \mathbf{C}_{\text{algo}} + 2D_C \widetilde{W} \mathbf{G}_{\text{algo}}. \quad (53)$$

Remark 6. The two last equivalent terms in equation (15) motivate two possible definitions for the algorithmic or time discrete directional derivative $(DC[\delta\phi])_{\text{algo}}$,

$$(DC[\delta\phi])_{\text{algo}} = \mathbf{G}_{\text{algo}} : (DC[\delta\phi])_{\text{algo}}; \quad (DC[\delta\phi])_{\text{algo}} = \mathbf{G}_{n+1/2} : (DC[\delta\phi])_{\text{algo}}, \quad (54)$$

with \mathbf{G}_{algo} defined in (52) (notice that $\mathbf{G}_{\text{algo}} \neq \mathbf{G}_{n+1/2}$). The definition in (54)_a satisfies the condition in equation (51)_c whereas that in (54)_b does not. Hence, the latter cannot be used for the design of an EM time integration scheme.

5.2. Discrete form of the balance laws and integrals in electro-dynamics

A similar procedure to that in Section 4.3.1 will be followed in order to verify that the proposed time integration scheme presented (47) possesses the conservation properties as presented in Sections 4.3.1 to 4.3.4.

5.2.1. Discrete form of the global form for conservation of linear momentum

Following a similar procedure to that in Section 4.3.1, taking $\delta\phi = \boldsymbol{\xi}$, with $\mathbb{R}^3 \ni \boldsymbol{\xi} = \text{const.}$ in \mathcal{W}_ϕ in (47)_b yields

$$\frac{\Delta \mathbf{L}}{\Delta t} - \mathbf{F}_{n+1/2}^{\text{ext}} = \mathbf{0}; \quad \mathbf{F}_{n+1/2}^{\text{ext}} = \int_{\partial_t \mathcal{B}_0} \mathbf{t}_{0_{n+1/2}} dA + \int_{\mathcal{B}_0} \mathbf{f}_{0_{n+1/2}} dV, \quad (55)$$

From equation (55) and for vanishing external forces $\mathbf{F}_{n+1/2}^{\text{ext}}$, it can be seen that the total linear momentum \mathbf{L} remains constant..

5.2.2. Discrete form of the global form for conservation of angular momentum

Taking $\delta\phi = \boldsymbol{\xi} \times \boldsymbol{\phi}_{n+1/2}$, with $\mathbb{R}^3 \ni \boldsymbol{\xi} = \text{const.}$ in \mathcal{W}_ϕ in (47)_b yields

$$\frac{\Delta \mathbf{J}}{\Delta t} - \mathbf{M}_{n+1/2}^{\text{ext}} = \mathbf{0}; \quad \mathbf{M}_{n+1/2}^{\text{ext}} = \int_{\partial_t \mathcal{B}_0} \boldsymbol{\phi}_{n+1/2} \times \mathbf{t}_{0_{n+1/2}} dA + \int_{\mathcal{B}_0} \boldsymbol{\phi}_{n+1/2} \times \mathbf{f}_{0_{n+1/2}} dV. \quad (56)$$

From equation (56) and for vanishing external torques $\mathbf{M}_{n+1/2}^{\text{ext}}$, it can be seen that the total angular momentum \mathbf{J} remains constant.

5.2.3. Discrete form of the global form for the Gauss law

Taking $\delta\varphi = \xi$, with $\mathbb{R} \ni \xi = \text{const.}$, the weak form \mathcal{W}_φ in (47) leads to

$$\int_{\mathcal{B}_0} \rho_{0_{n+1/2}}^e dV + \int_{\partial_\omega \mathcal{B}_0} \omega_{0_{n+1/2}}^e dA = 0. \quad (57)$$

For time independent volumetric and surface electrical charges ρ_0^e and ω_0^e , (57) shows that the total electrical charge is zero.

5.2.4. Discrete form of the global form for conservation of energy

In this section, a similar analysis to that in Section (4.3.4) will be presented for the semi-discrete weak forms in (47). For this purpose, we replace the test functions $\{\delta \mathbf{v}, \delta \boldsymbol{\phi}, \delta \varphi, \delta \mathbf{D}_0\}$ in (47) with $\{\Delta \mathbf{v}, \Delta \boldsymbol{\phi}, \Delta \varphi, \Delta \mathbf{D}_0\} \in \mathbb{V}_0^\phi \times \mathbb{V}_0^\phi \times \mathbb{V}_0^\varphi \times \mathbb{V}^{D_0}$. This yields

$$\begin{aligned}
& \int_{\mathcal{B}_0} \left(\mathbf{v}_{n+1/2} - \frac{\Delta \boldsymbol{\phi}}{\Delta t} \right) \cdot \rho_0 \Delta \mathbf{v} \, dV = 0; \\
& \int_{\mathcal{B}_0} \rho_0 \frac{\Delta \mathbf{v}}{\Delta t} \cdot \Delta \boldsymbol{\phi} \, dV + \int_{\mathcal{B}_0} \mathbf{S}_{\text{algo}} : \frac{1}{2} (DC[\Delta \boldsymbol{\phi}])_{\text{algo}} \, dV - \int_{\mathcal{B}_0} \mathbf{f}_0 \cdot \Delta \boldsymbol{\phi} \, dV - \int_{\partial_t \mathcal{B}_0} \mathbf{t}_0 \cdot \Delta \boldsymbol{\phi} \, dA = 0; \\
& \int_{\mathcal{B}_0} \mathbf{D}_{0_{n+1/2}} \cdot \nabla_0 \Delta \varphi \, dV + \int_{\mathcal{B}_0} \rho_{0_{n+1/2}}^e \Delta \varphi \, dV + \int_{\partial_\omega \mathcal{B}_0} \omega_{0_{n+1/2}}^e \Delta \varphi \, dA = 0; \\
& \int_{\mathcal{B}_0} \Delta \mathbf{D}_0 \cdot \left(D_{D_0} \widetilde{W} + \nabla_0 \varphi_{n+1/2} \right) \, dV = 0.
\end{aligned} \tag{58}$$

Consideration of time independent forces \mathbf{f}_0 and \mathbf{t}_0 and charges ρ_0^e and ω_0^e and after addition of the four equations in (58), it yields

$$\begin{aligned}
& \Delta K + \int_{\mathcal{B}_0} \left(\mathbf{S}_{\text{algo}} : \frac{1}{2} (DC[\Delta \boldsymbol{\phi}])_{\text{algo}} + D_{D_0} \widetilde{W} \cdot \Delta \mathbf{D}_0 \right) \, dV \\
& + \int_{\mathcal{B}_0} \mathbf{D}_{0_{n+1/2}} \cdot \nabla_0 \Delta \varphi \, dV + \int_{\mathcal{B}_0} \Delta \mathbf{D}_0 \cdot \nabla_0 \varphi_{n+1/2} \, dV - \Delta \Pi_{\text{ext}}^m(\boldsymbol{\phi}) - \Delta \Pi_{\text{ext}}^e(\varphi) = 0,
\end{aligned} \tag{59}$$

The third and fourth terms in above equation can be re-written as

$$\int_{\mathcal{B}_0} \mathbf{D}_{0_{n+1/2}} \cdot \nabla_0 \Delta \varphi \, dV + \int_{\mathcal{B}_0} \Delta \mathbf{D}_0 \cdot \nabla_0 \varphi_{n+1/2} \, dV = \int_{\mathcal{B}_0} \Delta (\mathbf{D}_0 \cdot \nabla_0 \varphi) \, dV. \tag{60}$$

From the definition of the algorithmic stress \mathbf{S}_{algo} in (53) and those for $(DC[\delta \boldsymbol{\phi}])_{\text{algo}}$, \mathbf{C}_{algo} and \mathbf{G}_{algo} in (52), it is possible to re-write the second term in (59)_b as

$$\begin{aligned}
\mathbf{S}_{\text{algo}} : \frac{1}{2} (DC[\Delta \boldsymbol{\phi}])_{\text{algo}} &= \left(D_C \widetilde{W} + D_G \widetilde{W} \times \mathbf{C}_{\text{algo}} + D_C \widetilde{W} \mathbf{G}_{\text{algo}} \right) : (DC[\Delta \boldsymbol{\phi}])_{\text{algo}} \\
&= D_C \widetilde{W} : \Delta \mathbf{C} + D_G \widetilde{W} : \Delta \mathbf{G} + D_C \widetilde{W} \Delta \mathbf{C}.
\end{aligned} \tag{61}$$

Substitution of 60 and (61) into (59) yields

$$\begin{aligned}
& \Delta K + \int_{\mathcal{B}_0} \left(D_C \widetilde{W} : \Delta \mathbf{C} + D_G \widetilde{W} : \Delta \mathbf{G} + D_C \widetilde{W} \Delta \mathbf{C} + D_{D_0} \widetilde{W} \cdot \Delta \mathbf{D}_0 \right) \, dV \\
& + \int_{\mathcal{B}_0} \Delta (\mathbf{D}_0 \cdot \nabla_0 \varphi) \, dV - \Delta \Pi_{\text{ext}}^m(\boldsymbol{\phi}) - \Delta \Pi_{\text{ext}}^e(\varphi) = 0.
\end{aligned} \tag{62}$$

Comparison of (62) and the definition of the total Hamiltonian $\mathcal{H}_{\widetilde{W}}$ in (44) enables to conclude that conservation of energy for the implicit one-step time integrator in equation (47) requires the directionality property in equation (49) to be satisfied. Two points have been crucial to arrive at this conclusion. First, the consideration of the algorithmic fields \mathbf{C}_{algo} and \mathbf{G}_{algo} in (52) has enabled to obtain the identity in equation (61). Second, the consideration of $\mathbf{D}_{0_{n+1/2}}$ (47)_c and of $\nabla_0 \varphi_{n+1/2}$ in (47)_d has been essential in order to re-write the third and fourth terms in (59) as in (60).

Remark 7. The stationary conditions in (37) lead us to propose an implicit one-step time integrator for the Helmholtz-based formulation as

$$\begin{aligned}
 (\mathcal{W}_v)_{\text{algo}} &= \int_{\mathcal{B}_0} \left(\mathbf{v}_{n+1/2} - \frac{\Delta \phi}{\Delta t} \right) \cdot \rho_0 \delta \mathbf{v} \, dV = 0; \\
 (\mathcal{W}_\phi)_{\text{algo}} &= \int_{\mathcal{B}_0} \rho_0 \frac{\Delta \mathbf{v}}{\Delta t} \cdot \delta \phi \, dV + \int_{\mathcal{B}_0} \mathbf{S}_{\text{algo}} : \frac{1}{2} (D\mathbf{C}[\delta \phi])_{\text{algo}} \, dV - \int_{\mathcal{B}_0} \mathbf{f}_{0_{n+1/2}} \cdot \delta \phi \, dV - \\
 &\quad \int_{\partial_t \mathcal{B}_0} \mathbf{t}_{0_{n+1/2}} \cdot \delta \phi \, dA = 0; \\
 (\mathcal{W}_\varphi)_{\text{algo}} &= - \int_{\mathcal{B}_0} D_{\mathbf{E}_0} \widetilde{W}_\phi \nabla_0 \delta \varphi \, dV + \int_{\mathcal{B}_0} \rho_{0_{n+1/2}}^e \delta \varphi \, dV + \int_{\partial_\omega \mathcal{B}_0} \omega_{0_{n+1+2}}^e \delta \varphi \, dA = 0,
 \end{aligned} \tag{63}$$

where \mathbf{S}_{algo} is given in (53). and where $\{D_{\mathbf{C}} \widetilde{W}_\phi, D_{\mathbf{G}} \widetilde{W}_\phi, D_C \widetilde{W}_\phi, D_{\mathbf{E}_0} \widetilde{W}_\phi\}$ represent the discrete derivatives of the Helmholtz functional $\widetilde{W}_\phi(\mathbf{C}, \mathbf{G}, C, \mathbf{E}_0)$ with respect to $\{\mathbf{C}, \mathbf{G}, C, \mathbf{E}_0\}$. Similarly to the time integrator in (47), we use a definition of the (multiple) discrete derivatives of $\widetilde{W}_\phi(\mathbf{C}, \mathbf{G}, C, \mathbf{E}_0)$ based on the generic definition followed in [19]. In this case, the discrete derivatives must satisfy the same properties as in Section 5.1.1, where now the directionality property is given by

$$D_{\mathbf{C}} \widetilde{W}_\phi : \Delta \mathbf{C} + D_{\mathbf{G}} \widetilde{W}_\phi : \Delta \mathbf{G} + D_C \widetilde{W}_\phi \Delta C + D_{\mathbf{E}_0} \widetilde{W}_\phi \cdot \Delta \mathbf{E}_0 = \Delta \widetilde{W}_\phi. \tag{64}$$

Note that identical results to those in Sections 5.2.1, 5.2.2 and 5.2.3 can be obtained for the weak forms in (63) regarding conservation of linear momentum, angular momentum, and the Gauss law, respectively. For the energy conservation, a similar result to that in (62) is also obtained

$$\begin{aligned}
 \Delta K + \int_{\mathcal{B}_0} \left(D_{\mathbf{C}} \widetilde{W}_\phi : \Delta \mathbf{C} + D_{\mathbf{G}} \widetilde{W}_\phi : \Delta \mathbf{G} + D_C \widetilde{W}_\phi \Delta C + D_{\mathbf{E}_0} \widetilde{W}_\phi \cdot \Delta \mathbf{E}_0 \right) \, dV \\
 - \Delta \Pi_{\text{ext}}^m(\phi) - \Delta \Pi_{\text{ext}}^e(\varphi) = 0.
 \end{aligned} \tag{65}$$

Comparison of (65) and the definition of the total Hamiltonian $\mathcal{H}_{\widetilde{W}_\phi}$ in (46) enables to conclude that conservation of energy for the implicit one-step time integrator in equation (63) requires the directionality property in equation (64) to be satisfied.

6. Finite Element implementation

As standard in finite elements, the domain \mathcal{B}_0 described in Section 2.1 and representing the EAP is sub-divided into a finite set of non-overlapping elements $e \in \mathbb{E}$ such that

$$\mathcal{B}_0 \approx \mathcal{B}_0^h = \bigcup_{e \in \mathbb{E}} \mathcal{B}_0^e. \tag{66}$$

The unknown fields $\{\mathbf{v}, \phi, \varphi, \mathbf{D}_0\}$ in the semi-discrete weak forms \mathcal{W}_v , \mathcal{W}_ϕ , \mathcal{W}_φ and $\mathcal{W}_{\mathbf{D}_0}$ in (47) are discretised employing the following functional spaces $\mathbb{V}^{\phi^h} \times \mathbb{V}^{\phi^h} \times \mathbb{V}^{\varphi^h} \times \mathbb{V}^{\mathbf{D}_0^h}$ defined as

$$\begin{aligned}
 \mathbb{V}^{\phi^h} &= \{\phi \in \mathbb{V}^\phi; \quad \phi^h|_{\mathcal{B}_0^e} = \sum_{a=1}^{n_{\text{node}}^\phi} N_a^\phi \phi_a\}; \\
 \mathbb{V}^{\varphi^h} &= \{\varphi \in \mathbb{V}^\varphi; \quad \varphi^h|_{\mathcal{B}_0^e} = \sum_{a=1}^{n_{\text{node}}^\varphi} N_a^\varphi \varphi_a\}; \\
 \mathbb{V}^{\mathbf{D}_0^h} &= \{\mathbf{D}_0 \in \mathbb{V}^{\mathbf{D}_0}; \quad \mathbf{D}_0^h|_{\mathcal{B}_0^e} = \sum_{a=1}^{n_{\text{node}}^{\mathbf{D}_0}} N_a^{\mathbf{D}_0} \mathbf{D}_{0a}\},
 \end{aligned} \tag{67}$$

where for any field $\mathbf{y} \in \{\phi, \varphi, \mathbf{D}_0\}$, $n_{\text{node}}^{\mathbf{y}}$ denotes the number of nodes per element of the discretisation associated with the field \mathbf{y} and $N_a^{\mathbf{y}} : \mathcal{B}_0^e \rightarrow \mathbb{R}$, the a^{th} shape function used for the interpolation of \mathbf{y} . In addition, \mathbf{y}_a represents the value of the field \mathbf{y} at the a^{th} node of a given finite element. Similarly, following a Bubnov-Galerkin approach, the functional spaces for the virtual variations $\{\delta \mathbf{v}, \delta \phi, \delta \varphi, \delta \mathbf{D}_0\} \in \mathbb{V}_0^{\phi^h} \times \mathbb{V}_0^{\varphi^h} \times \mathbb{V}_0^{\phi^h} \times \mathbb{V}^{\mathbf{D}_0^h}$ are defined as

$$\begin{aligned} \mathbb{V}_0^{\phi^h} &= \left\{ \forall \phi \in \mathbb{V}^{\phi^h}; \quad \phi = \mathbf{0} \text{ on } \partial_\phi \mathcal{B}_0 \right\}; \\ \mathbb{V}_0^{\varphi^h} &= \left\{ \forall \varphi \in \mathbb{V}^{\varphi^h}; \quad \varphi = 0 \text{ on } \partial_\varphi \mathcal{B}_0 \right\}. \end{aligned} \quad (68)$$

Even though the relation between the time derivative of ϕ and the velocity field \mathbf{v} is considered in a weak manner (refer to the weak form \mathcal{W}_v in (47)_a), the consideration of equal functional spaces for both fields, namely $\phi \in \mathbb{V}^\phi$ and $\mathbf{v} \in \mathbb{V}^\phi$ enables to conclude that equation (47)_a holds strongly, namely

$$\frac{\Delta \phi}{\Delta t} = \mathbf{v}_{n+1/2}. \quad (69)$$

Consideration of the functional spaces for $\{\mathbf{v}, \phi, \varphi, \mathbf{D}_0\}$ and $\{\delta \mathbf{v}, \delta \phi, \delta \varphi, \delta \mathbf{D}_0\}$ in (67) and (68) enables the last three weak forms \mathcal{W}_ϕ , \mathcal{W}_φ and $\mathcal{W}_{\mathbf{D}_0}$ in (47) to be written in terms of their associated elemental residual contributions, namely

$$\mathcal{W}_\phi = \sum_{e=1}^N \delta \phi_a \cdot \mathbf{R}_{a,e}^\phi; \quad \mathcal{W}_\varphi = \sum_{e=1}^N \delta \varphi_a R_{a,e}^\varphi; \quad \mathcal{W}_{\mathbf{D}_0} = \sum_{e=1}^N \delta \mathbf{D}_{0a} \cdot \mathbf{R}_{a,e}^{\mathbf{D}_0}, \quad (70)$$

where N denotes the number of elements for the underlying discretisation. Each of the residual contributions $\mathbf{R}_{a,e}^\phi$, $R_{a,e}^\varphi$ and $\mathbf{R}_{a,e}^{\mathbf{D}_0}$ can be expressed as⁶

$$\begin{aligned} \mathbf{R}_{a,e}^\phi &= \int_{\mathcal{B}_0^e} \rho_0 N_\phi^a \left(2 \frac{\Delta \phi}{\Delta t^2} - 2 \frac{\mathbf{v}_n}{\Delta t} \right) dV + \int_{\mathcal{B}_0^e} (\mathbf{F}_{n+1/2} \mathbf{S}_{\text{algo}}) \nabla_0 N_\phi^a dV + \int_{\mathcal{B}_0^e} N_\phi^a \mathbf{f}_{0_{n+1/2}} dV; \\ R_{a,e}^\varphi &= \int_{\mathcal{B}_0^e} \mathbf{D}_{0_{n+1/2}} \cdot \nabla_0 N_\varphi^a dV + \int_{\mathcal{B}_0^e} N_\varphi^a \rho_{0_{n+1/2}}^e dV; \\ \mathbf{R}_{a,e}^{\mathbf{D}_0} &= \int_{\mathcal{B}_0^e} N_a^{\mathbf{D}_0} \left(D_{\mathbf{D}_0} \widetilde{\mathbf{W}} + \nabla_0 \varphi_{n+1/2} \right) dV. \end{aligned} \quad (71)$$

where use of equation (69) has been made of in the inertial term of the residual $\mathbf{R}_{a,e}^\phi$ in (71)_a. A consistent linearisation of the nonlinear residual contributions (71) has been used in this work. Finally, in order to reduce the computational cost of the proposed formulation, a piecewise discontinuous interpolation of the field \mathbf{D}_0 is followed. A standard static condensation procedure [37, 9] is used to condense out the degrees of freedom of the field \mathbf{D}_0 , yielding a formulation with a cost comparable to that of a two-field $\{\phi, \varphi\}$ formulation.

7. Numerical examples

The objective of this section is to study the performance of the newly proposed (internal energy-based) EM time integration scheme presented in equation (47) in a variety of examples.

⁶For simplicity, the external contributions on the boundary of the continuum and associated with \mathbf{t}_0 and ω_0^e have not been included in (71).

7.1. Numerical example 1

The objective of this example is:

- O1.I** Study of the accuracy of the proposed EM time integration scheme given in equation (47). Specifically, the objective is to verify the mathematical conclusion obtained in Appendix A, according to which the proposed EM time integration scheme must converge at the same (second order) rate as the midpoint-rule integrator.

The geometry and the boundary conditions for the actuator considered in this example are depicted in Figure 2 and Table 1. The actuator is free in space. An initial velocity \mathbf{v}_0 is given by

$$\mathbf{v}_0 = \boldsymbol{\omega} \times \mathbf{X}; \quad \boldsymbol{\omega} = [0, 0, 10]^T s^{-1}; \quad \mathbf{X} = [X_1, X_2, X_3]^T, \quad (72)$$

with $\{X_1, X_2, X_3\}$ aligned with the orthonormal basis $\{\mathbf{e}_1, \mathbf{e}_2, \mathbf{e}_3\}$, respectively (see Figure 2). Electrical Dirichlet boundary conditions are applied on top and bottom of the plate. Specifically, a value of the potential $\varphi = 0 V$ is applied on the top (blue) electrode and of $\varphi = 100 KV$ on the bottom (blue) electrode (refer to Figure 2).

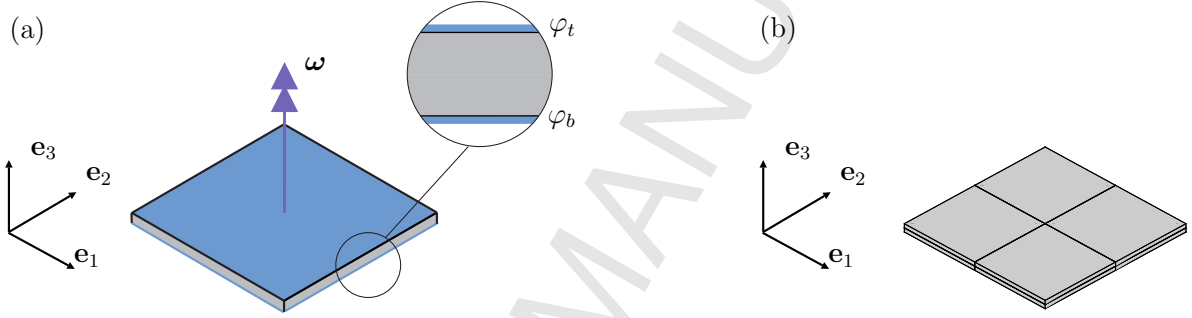


Figure 2: Numerical example 1. (a) Configuration and boundary conditions; (b) discretisation considered: hexahedral mesh with 8 elements and $\{243, 81, 192\}$ degrees of freedom for $\{\phi, \varphi, \mathbf{D}_0\}$. Interpolation spaces for $\{\phi, \varphi, \mathbf{D}_0\}$ are $Q2^C-Q2^C-Q1^D$, where C and D denote continuous or discontinuous interpolation across elements.

The purely mechanical contribution of the constitutive model considered corresponds to that of a Mooney-Rivlin model (refer to equation (19)). The electromechanical component corresponds to that of an ideal dielectric elastomer (see equation (18)). The material parameters of the constitutive model can be found in Table 1.

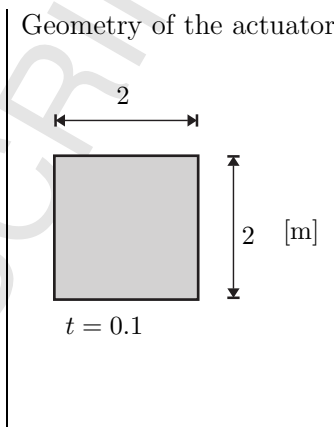
The discretisation shown in Figure 2b has been used in this example, comprised of 8 hexahedral elements. A continuous serpenpedit-type $Q2$ interpolation has been used for the fields $\{\phi, \varphi\}$ and a discontinuous trilinear $Q1$ interpolation has been used for \mathbf{D}_0 .

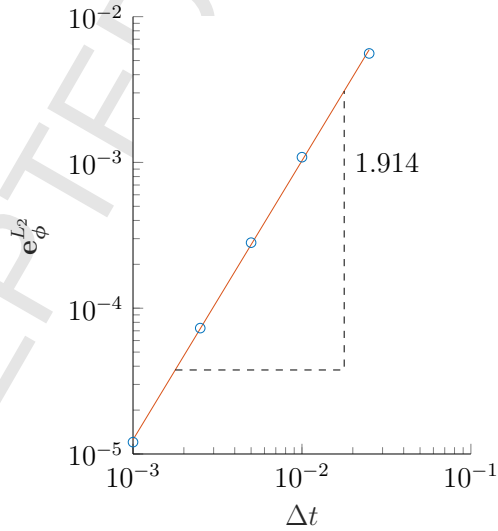
In relation to objective **O1.I**, a study of the accuracy of the proposed EM time integrator in (47) has been carried out. This is shown in Figure 3, which depicts the convergence with respect to time of the solution when using the hexahedral finite element described above. Specifically, for the mesh depicted in Figure 2, the L^2 norm of the error between the solution obtained with five different time steps $\{\Delta t_1, \dots, \Delta t_5\}$ such that $\Delta t_1 = 2.5e-2$, $\Delta t_2 = 1e-2$, $\Delta t_3 = 5e-3$, $\Delta t_4 = 2.5e-3$, $\Delta t_5 = 1e-3$ and that obtained with a reference time step Δt_{ref} such that $\Delta t_{\text{ref}} \ll \Delta t_5$ has been computed. To be specific, the L^2 of the error for the field ϕ , denoted as $e_\phi^{L^2}$ is computed as

$$e_\phi^{L^2} = \frac{\|\phi - \phi_{\text{ref}}\|_{L^2}}{\|\phi_{\text{ref}}\|_{L^2}}; \quad \|\phi\|_{L^2} = \left[\int_{B_0} (\phi \cdot \phi) dV \right]^{\frac{1}{2}}, \quad (73)$$

where $(\bullet)_{\text{ref}}$ denotes the solution for the field \bullet obtained by means of the reference time step size Δt_{ref} . A time-interval of 0.1 seconds has been considered in order to carry out the described convergence study. Crucially, Figure 3 proves that the proposed EM time integrator is second order accurate in time (slope of 1.914).

Table 1: Numerical example 1. Material parameters, simulation parameters and geometry.

Mechanical parameters	μ_1	5×10^4	Pa	Geometry of the actuator 
	μ_2	1×10^5	Pa	
	λ	4×10^4	Pa	
Electrical parameters	ϵ_0	8.854×10^{-12}	$\text{A}^2 \text{s}^4 \text{kg}^{-1} \text{m}^{-3}$	
	ϵ_r	5	–	
Ref. potential	φ_0	0	V	
El. potential at $X_3 = 0.1$	φ_t	10^5	V	
El. potential at $X_3 = 0$	φ_b	0	V	
Density	ρ_0	900	kg m^{-3}	
Simulation time	T	0.1	s	
Reference time-step size	Δt_{ref}	10^{-4}	s	
Newton tolerance	ϵ	10^{-6}	J	

Figure 3: Numerical example 1. Second order (1.914) accuracy of the proposed EM time integration scheme in (47) with respect to time for the field ϕ . Results obtained for hexahedral $Q2^C$ - $Q2^C$ - $Q1^D$ element.

7.2. Numerical example 2

The objective of this example is two-fold:

- O2.I** Comparison of the performance of two families of finite elements. Specifically, a tetrahedral-based and an hexahedral-based finite elements will be considered. The interpolation spaces for the fields $\{\phi, \varphi, \mathbf{D}_0\}$ will be carried out in accordance to Table 2.
- O2.II** Assessment of the thermodynamical consistency of the time integration scheme presented in (47) for both families of finite elements. In particular, the conservation properties of the proposed time EM time integration scheme will be analysed.

Discretisation in space		
Fields	Tet-based	Hex-based
ϕ	$P2^C$	$Q2^C$
φ	$P2^C$	$Q2^C$
\mathbf{D}_0	$P1^D$	$Q1^D$

Table 2: Numerical example 2. Discretisation spaces for tetrahedral-based and hexahedral-based finite elements considered. The superscripts C and D stand for continuous and discontinuous interpolations of fields $\{\phi, \varphi, \mathbf{D}_0\}$.

The geometry and boundary conditions for the actuator considered in this example are described in Figure 4 and Table 3. The actuator is clamped on one side (zero Dirichlet displacement boundary conditions). A surface electrical charge ω_0^e is applied on the top (purple) electrode (refer to Figure 4) whereas a prescribed value of the electric potential of $\varphi = 0 V$ is applied on the bottom (blue) electrode. The time dependent function ω_0^e is given by

$$\omega_0^e = 10^{-3} \times \begin{cases} \sin\left(\frac{0.5\pi}{0.4s} t\right) & \text{for } t \leq 0.4 \text{ s} \\ 1 & \text{for } 0.4 \text{ s} < t \leq 1.0 \text{ s} \\ \cos\left(\frac{0.5\pi}{1.4s-1.0s} (t-1 \text{ s})\right) & \text{for } 1.0 \text{ s} < t \leq 1.4 \text{ s} \\ 0 & \text{for } t > 1.4 \text{ s} \end{cases} [Q/m^2]. \quad (74)$$

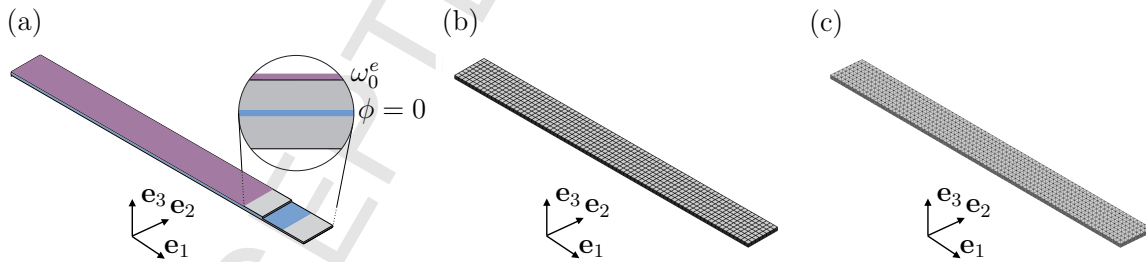


Figure 4: Numerical example 2. (a) Configuration and boundary conditions. Discretisations considered: (b) hexahedral mesh with $\{40203, 13401, 61440\}$ degrees of freedom for $\{\phi, \varphi, \mathbf{D}_0\}$; (c) tetrahedral mesh with $\{55899, 18633, 130584\}$ degrees of freedom for $\{\phi, \varphi, \mathbf{D}_0\}$. Interpolation spaces for $\{\phi, \varphi, \mathbf{D}_0\}$ are provided by Table 2.

The purely mechanical contribution of the constitutive model considered corresponds to that of a Mooney-Rivlin model (refer to equation (19)). The electromechanical component corresponds to that of an ideal dielectric elastomer (see equation (18)). The material parameters of the constitutive model can be found in Table 3.

With regards to **O2.I**, two discretisations are considered, one for each of the two families of finite elements described in Table 2. Both hexahedral-based and tetrahedral-based meshes are

Table 3: Numerical example 2. Material parameters, simulation parameters and geometry.

Mechanical parameters	μ_1	5×10^4	Pa	<p>Geometry of the actuator</p> <p>0.1</p> <p>1 [m]</p> <p>$t = 0.01$</p>
	μ_2	1×10^5	Pa	
	λ	1×10^5	Pa	
Electrical parameters	ϵ_0	8.854×10^{-12}	$A^2 s^4 kg^{-1} m^{-3}$	
	ϵ_r	3	—	
Ref. potential	ϕ_0	0	V	
Max. surface charge	ω_0	1×10^{-3}	Q/m^2	
Density	ρ_0	1000	$kg m^{-3}$	
Timestep size	Δt	0.02	s	
Simulation time	T	4	s	
Newton tolerance	ϵ	10^{-5}	J	

represented in Figure 4_b and 4_c, respectively. The mesh associated with the hexahedral-based discretisation has 2,560 elements, 13,401 nodes for both fields $\{\phi, \varphi\}$ ($\{40203, 13401\}$ degrees of freedom associated to each field) and 20,480 nodes for \mathbf{D}_0 (61,440 degrees of freedom). The mesh associated with the tetrahedral-based discretisation has 10,882 elements, 18,633 nodes for both fields $\{\phi, \varphi\}$ ($\{55899, 18633\}$ degrees of freedom associated to each field) and 43,528 nodes for \mathbf{D}_0 (130,584 degrees of freedom). In both cases, \mathbf{D}_0 is interpolated using a discontinuous interpolation across elements, which allows to condense out this field.

Figure 5 shows the contour plot distribution of the von Mises stress for the hexahedral-based discretisation for different time steps. Figure 6 shows the contour plot distribution of the von Mises stress for the tetrahedral-based discretisation for different time steps. A good agreement is observed between both discretisations in terms of the final configuration (displacements) as well as the stress distribution.

Regarding objective **O2.II**, Figure 7 shows the evolution of the Hamiltonian $\mathcal{H}_{\tilde{W}}$ (44) using both hexahedral and tetrahedral discretisations for a given time step size of $\Delta t = 0.02$ s. The evolution of $\mathcal{H}_{\tilde{W}}$ is exactly identical for both discretisations. Crucially, $\mathcal{H}_{\tilde{W}}$ remains constant for the time interval $[0.4, 1] \cup [1.4, 4]$, namely, when the surface charge ω_0^e in equation (74) remains constant, proving that the Hamiltonian is conserved in that range. This can be more clearly appreciated in Figure 8, where the variation $\Delta \mathcal{H}_{\tilde{W}} = \mathcal{H}_{\tilde{W}_{n+1}} - \mathcal{H}_{\tilde{W}_n}$ is depicted for the aforementioned time interval. Crucially, the maximum value of $|\Delta \mathcal{H}_{\tilde{W}}|$ is always bounded below the user-defined Newton tolerance ϵ , which for this case was selected as $\epsilon = 10^{-5}$ (refer to Table 3).

7.3. Numerical example 3

The objective of this example is two-fold:

- O3.I** Comparison of the stability and robustness of the proposed EM time integration scheme against the midpoint-rule integrator.
- O3.II** Comparison of the thermodynamical consistency of the proposed time integrator to that of the midpoint-rule time integrator.
- O3.III** Verification of consistent angular momentum approximation.

The geometry and boundary conditions for the actuator considered in this example are described in Figure 9 and Table 4. The actuator is completely free (no Dirichlet boundary conditions are considered for the field ϕ). An initial velocity \mathbf{v}_0 is prescribed and given by

$$\mathbf{v}_0 = \boldsymbol{\omega} \times \mathbf{X}; \quad \boldsymbol{\omega} = [0, 0, 4]^T s^{-1}; \quad \mathbf{X} = [X_1, X_2, X_3]^T, \quad (75)$$

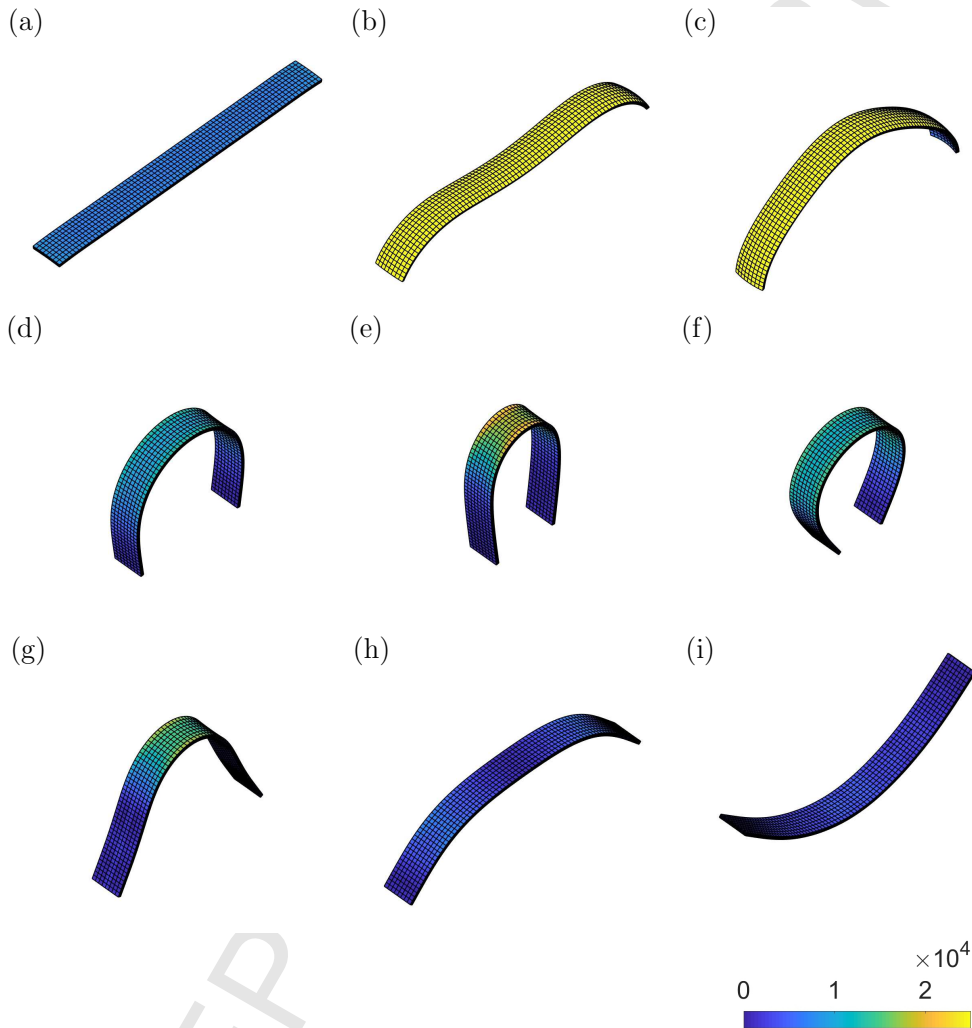


Figure 5: Numerical example 2. Contour plot of Von Mises stress for the hexahedral-based discretisation for different configurations corresponding to (left to right-top to bottom): (a) $t = 0 s$; (b) $t = 0.5 s$; (c) $t = 1 s$; (d) $t = 1.5 s$; (e) $t = 2 s$; (f) $t = 2.5 s$; (g) $t = 3 s$; (h) $t = 3.5 s$; (i) $t = 4 s$. Hexahedral mesh with $\{40203, 13401, 61440\}$ degrees of freedom for $\{\phi, \varphi, \mathbf{D}_0\}$. Interpolation spaces for $\{\phi, \varphi, \mathbf{D}_0\}$ are provided in Table 2.

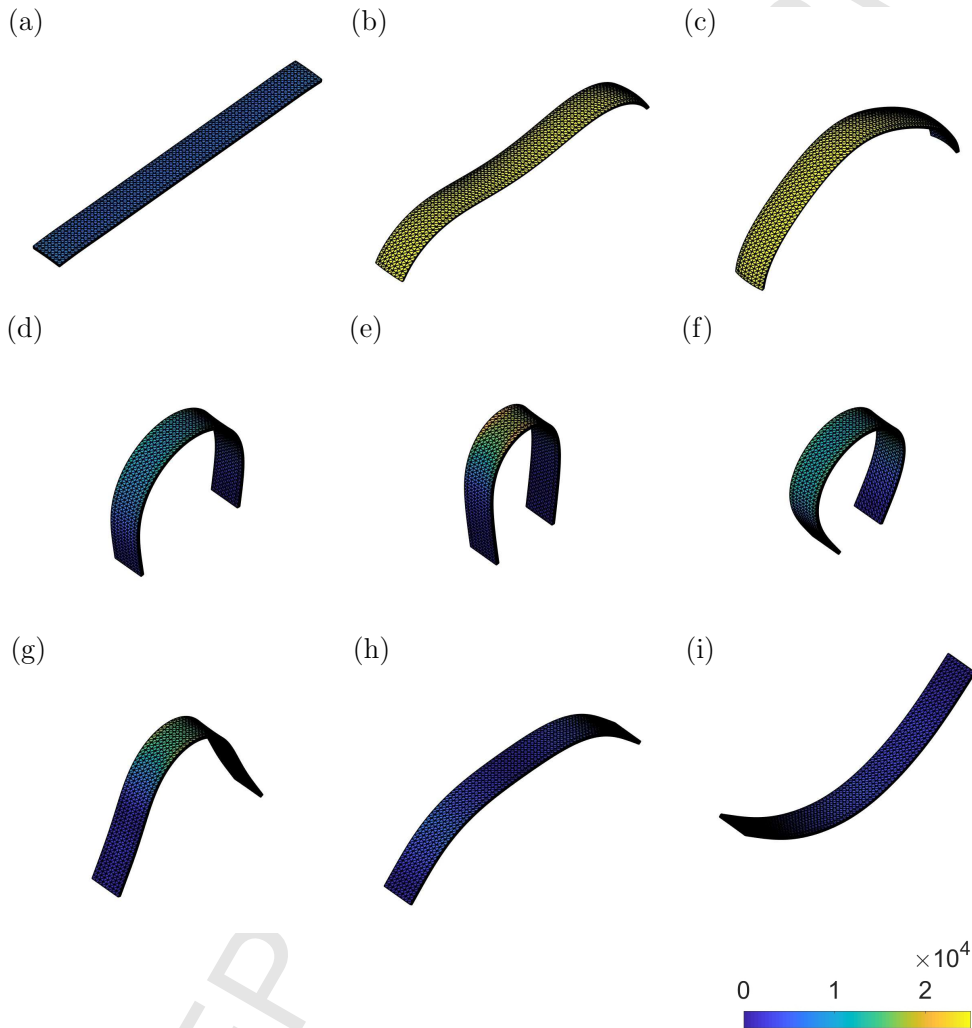


Figure 6: Numerical example 2. Contour plot of Von Mises stress for the tetrahedral-based discretisation for different configurations corresponding to (left to right-top to bottom): (a) $t = 0 s$; (b) $t = 0.5 s$; (c) $t = 1 s$; (d) $t = 1.5 s$; (e) $t = 2 s$; (f) $t = 2.5 s$; (g) $t = 3 s$; (h) $t = 3.5 s$; (i) $t = 4 s$. (c) Tetrahedral mesh with $\{55899, 18633, 130584\}$ degrees of freedom for $\{\phi, \varphi, \mathbf{D}_0\}$. Interpolation spaces for $\{\phi, \varphi, \mathbf{D}_0\}$ in Table 2.

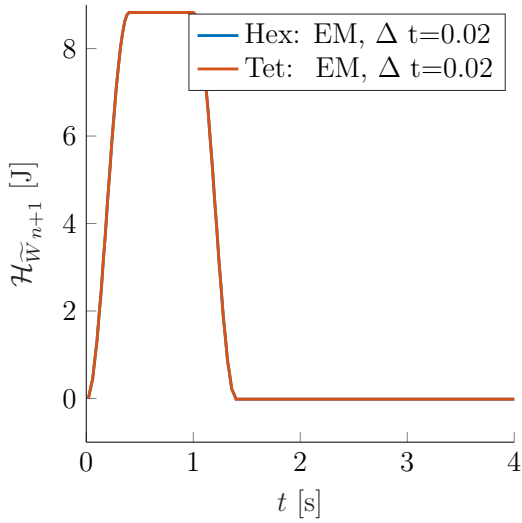


Figure 7: Numerical example 2. Time evolution of $\mathcal{H}_{\tilde{W}}$ for both hexahedral and tetrahedral discretisations using the proposed EM time integration scheme.

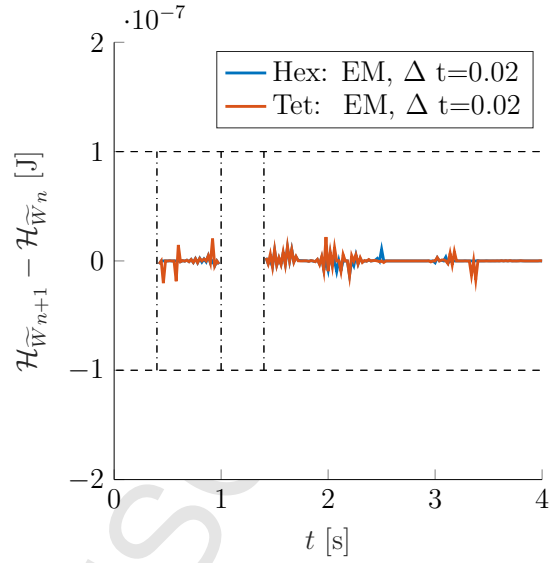


Figure 8: Numerical example 2. Time evolution of $\Delta\mathcal{H}_{\tilde{W}}$ for time interval $(0.4, 1) \cup [1.4, 4]$ for hexahedral and tetrahedral elements with proposed EM scheme.

with $\{X_1, X_2, X_3\}$ aligned with the orthonormal basis $\{e_1, e_2, e_3\}$, respectively (see Figure 9). A constant value for the electric potential of $\varphi = 0\text{ V}$ is applied on the blue electrode. A surface electric charge ω_0^e is applied on the purple electrode (see detailed view in Figure 9). The time dependent function ω_0^e is given by

$$\omega_0^e = (5 \times 10^{-3}) \times \begin{cases} \sin\left(\frac{0.5\pi}{0.4\text{s}} t\right) & \text{for } t \leq 0.4\text{ s} \\ 1 & \text{for } 0.4\text{ s} < t \leq 3.0\text{ s} \\ \cos\left(\frac{0.5\pi}{3.4\text{s}-3.0\text{s}} (t-3\text{ s})\right) & \text{for } 3.0\text{ s} < t \leq 3.4\text{ s} \\ 0 & \text{for } t > 3.4\text{ s} \end{cases} \quad [Q/m^2]. \quad (76)$$

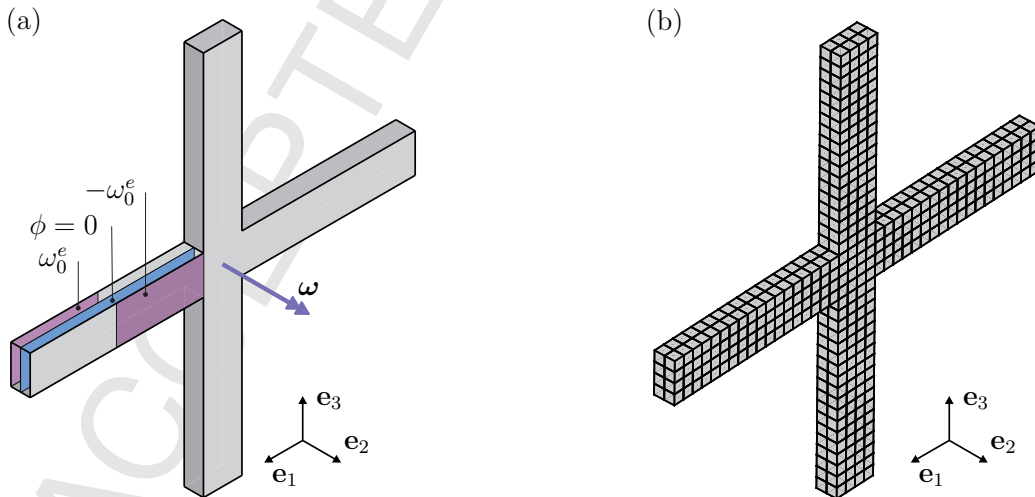
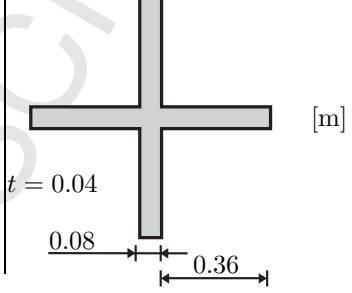


Figure 9: Numerical example 3. (a) Configuration and boundary conditions; (b) discretisation considered: hexahedral mesh with $\{13215, 4405, 16128\}$ degrees of freedom for $\{\phi, \varphi, \mathbf{D}_0\}$. Interpolation spaces $Q2^C$ - $Q2^C$ - $Q1^D$.

The constitutive model is the same as that used in the two preceding examples with the material parameters defined in Table 4. The discretisation shown in Figure 9_b has been used

in this example. Specifically, a total of 672 hexahedral $Q2^C$ - $Q2^C$ - $Q1^D$ finite elements have been considered, yielding a total number of degrees of freedom of $\{13215, 4405, 16128\}$ for the fields $\{\phi, \varphi, \mathbf{D}_0\}$.

Table 4: Numerical example 3. Material parameters, simulation parameters and geometry.

Mechanical parameters	μ_1	5×10^4	Pa	Geometry of the cross 
	μ_2	1×10^5	Pa	
	λ	5×10^5	Pa	
Electrical parameters	ϵ_0	8.854×10^{-12}	$\text{A}^2 \text{s}^4 \text{kg}^{-1} \text{m}^{-3}$	
	ϵ_r	4	N/V^2	
Ref. potential	ϕ_0	0	V	
Max. surface charge	ω_0	5×10^{-3}	Q/m^2	
Density	ρ_0	1000	kg m^{-3}	
Timestep size	Δt	0.01	s	
Simulation time	T	10	s	
Newton tolerance	ϵ	10^{-5}	J	

Regarding objective **O3.I**, Figure 10 shows that the midpoint-rule time integrator exhibits an energy blow-up and becomes unstable approximately in the interval $1 < t < 2$. However, the newly proposed EM time integrator remains stable for the whole simulation for the same fixed time step size of $\Delta t = 0.01 \text{ s}$. This proves that the proposed scheme is more robust and stable than the classical midpoint-rule.

In relation to objective **O3.II**, Figure 10 shows the evolution of $\mathcal{H}_{\bar{W}}$ for both the proposed EM time integrator and the midpoint-rule. Crucially, $\mathcal{H}_{\bar{W}}$ remains constant when using the proposed EM scheme for the time interval $[0.4, 3] \cup [3.4, 10]$, namely, when the surface charge ω_0^e in equation (76) remains constant, proving that the Hamiltonian is conserved in that range. This can be more clearly appreciated in Figure 11, where the variation $\Delta \mathcal{H}_{\bar{W}} = \mathcal{H}_{\bar{W}_{n+1}} - \mathcal{H}_{\bar{W}_n}$ is depicted for the aforementioned time interval. Crucially, the maximum value of $|\Delta \mathcal{H}_{\bar{W}}|$ is always bounded below the user-defined Newton tolerance ϵ , which for this case was selected as $\epsilon = 10^{-5}$ (refer to Table 4).

A clearer evolution of the energy blow-up for the midpoint-rule can be appreciated in Figure 12. For the interval $1 < t < 2$, a diverging pattern is observed in the evolution of the Hamiltonian for the midpoint-rule integrator which ends in an energy blow-up.

Additionally, in relation to objective **O3.III** Figure 13 shows the evolution of the norm of the total angular momentum \mathbf{J} of the system for both the proposed EM time integrator and the midpoint-rule (before the latter becomes unstable). Crucially, $\|\mathbf{J}\|$ remains constant when using the proposed EM scheme for the whole simulation, proving that the \mathbf{J} is conserved. This can be more clearly appreciated in Figure 14, where the variation $\Delta \|\mathbf{J}\| = \|\mathbf{J}_{n+1}\| - \|\mathbf{J}_n\|$ is depicted for the whole simulation. Crucially, the maximum value of $\Delta \|\mathbf{J}\|$ is also always bounded below the user-defined Newton tolerance ϵ (here $\epsilon = 10^{-5}$, refer to Table 4).

Finally, the contour plot distribution for the electric potential φ and the evolution of the combined rotation and electrically induced deformation in the actuator is depicted in Figure 15 for difference instances of time.

7.4. Numerical example 4

The objective of this example is:

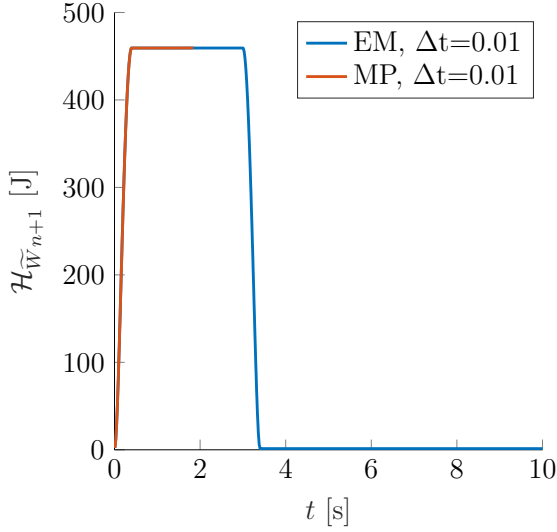


Figure 10: Numerical example 3. Time evolution of $\mathcal{H}_{\tilde{W}}$ with the proposed EM scheme and the midpoint-rule. Energy blow-up for midpoint-rule within time interval $4 < t < 6$.

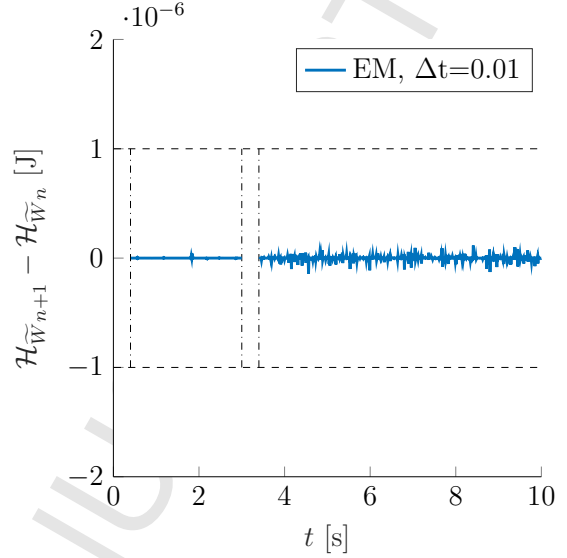


Figure 11: Numerical example 3. Time evolution of $\Delta\mathcal{H}_{\tilde{W}}$ in the time interval $[0.4, 3] \cup [3.4, 10]$ for hexahedral element with the proposed scheme.

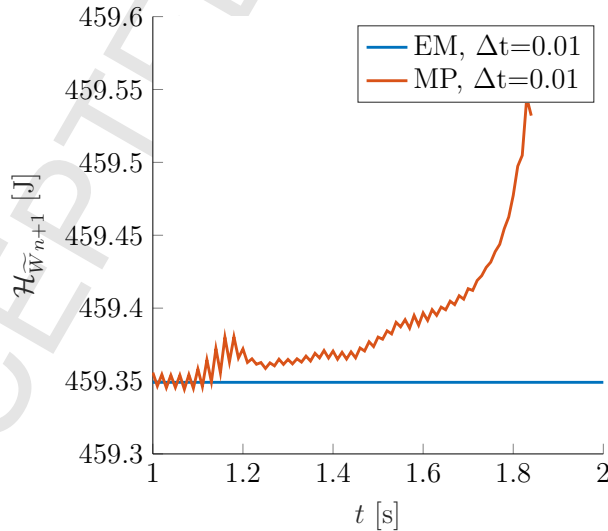


Figure 12: Numerical example 3. Time evolution of $\Delta\mathcal{H}_{\tilde{W}}$ in the time interval $1 < t < 2$ for hexahedral element. Energy blow-up of the midpoint-rule time integrator. Conservation of the Hamiltonian for proposed scheme.

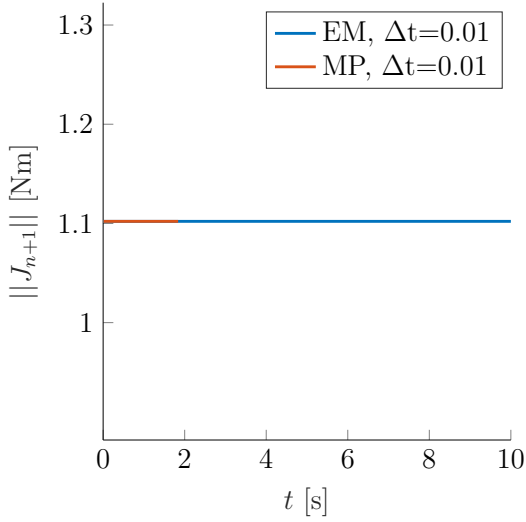


Figure 13: Numerical example 3. Time evolution of $\|\mathbf{J}\|$ with proposed EM scheme and midpoint-rule.

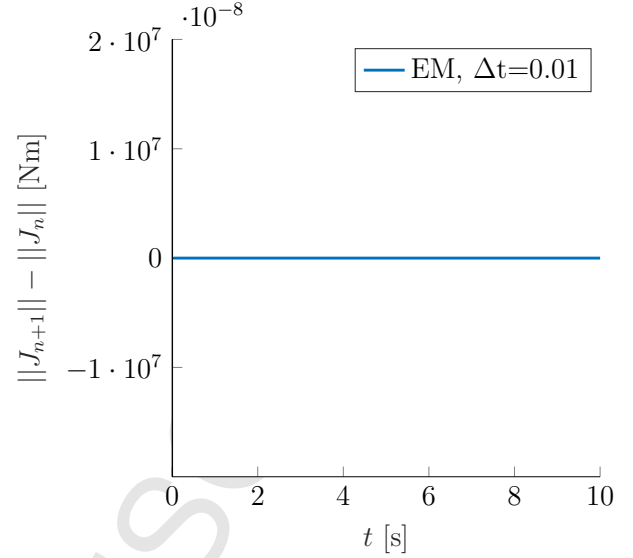


Figure 14: Numerical example 3. Time evolution of $\Delta\|\mathbf{J}\|$ for hexahedral element with proposed scheme.

O4.I The consideration of more sophisticated constitutive models allowing for the consideration of anisotropic effects. A comparison of the stability and robustness between the proposed EM time integrator and the midpoint-rule integrator will also be carried out in this example.

The geometry and boundary conditions for the actuator considered in this example are described in Figure 16 and Table 5. The actuator is clamped on one side (zero Dirichlet displacement boundary conditions). A surface electrical charge ω_0^e is applied on the purple electrode (refer to detailed view in Figure 16) whereas a prescribed value of the electric potential of $\varphi = 0\text{ V}$ is applied on the blue electrode (see detailed view in Figure 16). The time dependent function ω_0^e is given by

$$\omega_0^e = (2 \times 10^{-3}) \times \begin{cases} \sin\left(\frac{0.5\pi}{0.5\text{s}} t\right) & \text{for } t \leq 0.5\text{ s} \\ 1 & \text{for } 0.5\text{ s} < t \leq 1\text{ s} \\ \cos\left(\frac{0.5\pi}{1.5\text{s}-1\text{s}} (t - 1\text{ s})\right) & \text{for } 1\text{ s} < t \leq 1.5\text{ s} \\ 0 & \text{for } t > 1.5\text{ s} \end{cases} [Q/m^2]. \quad (77)$$

Regarding the constitutive model, its electromechanical component corresponds to that of an ideal dielectric elastomer (see equation (18)). The purely mechanical contribution is more complex than that considered in the preceding examples. This can be additively decomposed into purely isotropic and transversely anisotropic parts, namely

$$\widetilde{W}_m(\mathbf{C}, \mathbf{G}, C) = \widetilde{W}_m^{\text{iso}}(\mathbf{C}, \mathbf{G}, C) + \widetilde{W}_m^{\text{aniso}}(\mathbf{C}, \mathbf{G}, C). \quad (78)$$

In this example, the isotropic contribution $\widetilde{W}_m^{\text{iso}}(\mathbf{C}, \mathbf{G}, C)$ will be taken exactly as that a Mooney-Rivlin model (refer to equation (19)). The anisotropic contribution is defined based on Reference [45] as

$$\widetilde{W}_m^{\text{aniso}}(\mathbf{C}, \mathbf{G}, C) = \frac{\mu_3}{g_C + 1} (\text{tr}(\mathbf{C} \mathbf{M}))^{g_C + 1} + \frac{\mu_3}{g_G + 1} (\text{tr}(\mathbf{G} \mathbf{M}))^{g_G + 1} + \frac{\mu_3}{g_C} C^{-g_C}; \quad \mathbf{M} = \mathbf{N}_0 \otimes \mathbf{N}_0, \quad (79)$$

where the material parameters $\mu_3 > 0$, $g_C > 0$, $g_G > 0$ and $g_C \geq 1$ for this model can be found in Table 5. In addition, in above equation (79) \mathbf{N}_0 represents the preferred direction of anisotropy in the material configuration. In this example, \mathbf{N}_0 is defined as $\mathbf{N}_0 = [0.320 \quad -0.9712 \quad 0.320]^T$.

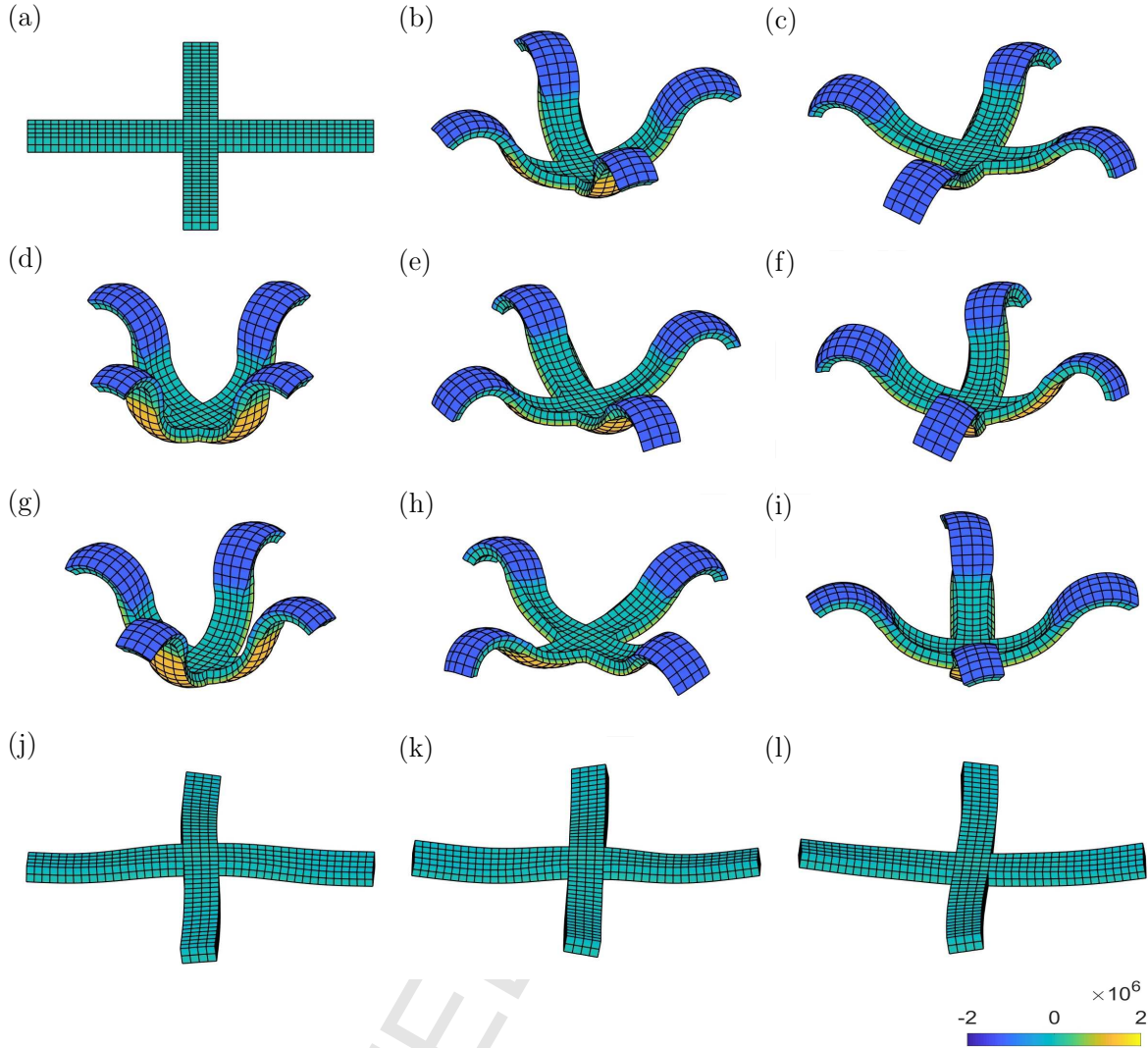


Figure 15: Numerical example 3. Contour plot of electric potential φ for hexahedral element for different configurations corresponding to (left to right-top to bottom): (a) $t = 0$ s; (b) $t = 0.4$ s; (c) $t = 0.8$ s; (d) $t = 1.2$ s; (e) $t = 1.6$ s; (f) $t = 2$ s; (g) $t = 2.4$ s; (h) $t = 2.8$ s; (i) $t = 3.2$ s; (j) $t = 3.6$ s; (k) $t = 4$ s; (l) $t = 4.4$ s.

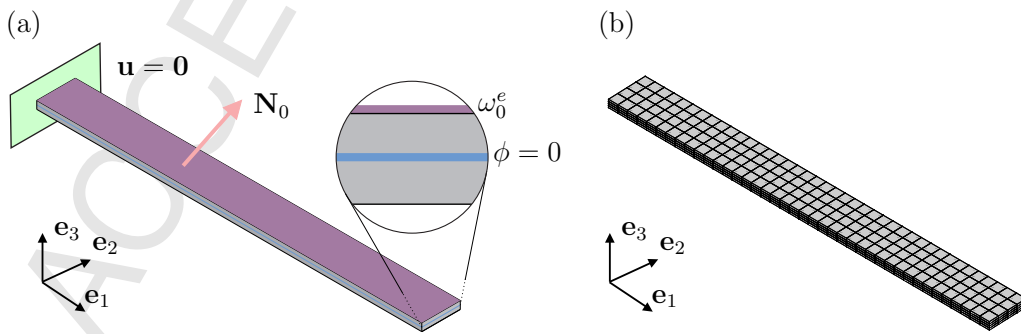
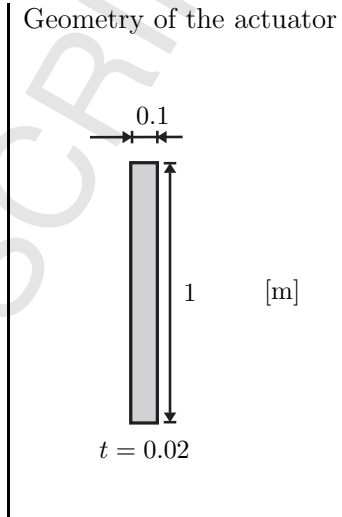


Figure 16: Numerical example 4. (a) Configuration and boundary conditions; (b) discretisation considered: hexahedral mesh with $\{10995, 3665, 15360\}$ degrees of freedom for $\{\phi, \varphi, \mathbf{D}_0\}$. Interpolation spaces $Q2^C$ - $Q2^C$ - $Q1^D$.

The discretisation shown in Figure 16_b has been used in this example. Specifically, a total of 640 hexahedral $Q2^C$ - $Q2^C$ - $Q1^D$ finite elements have been considered, yielding a total number of degrees of freedom of $\{10995, 3665, 15360\}$ for the fields $\{\phi, \varphi, \mathbf{D}_0\}$.

Table 5: Numerical example 4. Material parameters, simulation parameters and geometry.

Mechanical parameters	μ_1	5×10^4	Pa	Geometry of the actuator 
	μ_2	1×10^5	Pa	
	λ	1×10^6	Pa	
	μ_3	3×10^5	Pa	
	g_C	4	-	
	g_G	8	-	
Electrical parameters	g_C	1	-	
	ϵ_0	8.854×10^{-12}	$A^2 s^4 kg^{-1} m^{-3}$	
	ϵ_r	4	-	
Ref. potential	ϕ_0	0	V	
Max. surface charge	ω_0	2×10^{-3}	Q/m^2	
Density	ρ_0	1000	$kg m^{-3}$	
Timestep size	Δt	0.0025	s	
Simulation time	T	7.5	s	
Newton tolerance	ϵ	10^{-5}	J	

Regarding objective **O4.I**, Figure 17 shows that the midpoint-rule time integrator exhibits an energy blow-up and becomes unstable approximately in the interval $4 < t < 5$. However, the proposed time integrator remains stable for the whole simulation for the same fixed time step size of $\Delta t = 0.0025$ s. Like in the preceding example, where a simpler constitutive law was used, this proves that the proposed scheme is more robust and stable than the classical midpoint-rule. In addition, 17 shows the evolution of $\mathcal{H}_{\widetilde{W}}$ for both the proposed EM time integrator and the midpoint-rule (before the latter becomes unstable). Crucially, $\mathcal{H}_{\widetilde{W}}$ remains constant when using the proposed EM scheme for the time interval $[0.5, 1] \cup [1.5, 7.5]$, namely, when the surface charge ω_0^e in equation (77) remains constant, proving that the Hamiltonian is conserved in that range. This can be more clearly appreciated in Figure 18, where the variation $\Delta \mathcal{H}_{\widetilde{W}} = \mathcal{H}_{\widetilde{W}_{n+1}} - \mathcal{H}_{\widetilde{W}_n}$ is depicted for the aforementioned time interval. The maximum value of $|\Delta \mathcal{H}_{\widetilde{W}}|$ is always bounded below the user-defined Newton tolerance ϵ (refer to Table 5).

Finally, the contour plot distribution for the von Mises stress and the evolution of the electrically induced deformation in the actuator is depicted in Figure 19 for different instances of time.

7.5. Numerical example 5

The objective of this example is:

- O5.I** Comparison of the robustness between the proposed EM time integrator and the midpoint-rule time integrator in scenarios with more sophisticated electrically induced configurations which can represent a real challenge from the robustness standpoint of the algorithm.

The geometry and boundary conditions for the actuator considered in this example are very similar to those considered in Reference [43] and are described in Figure 20 and Table 6. The actuator is fully clamped on the perimeter of the blue electrode (see detailed view in Figure 20). A surface electrical charge ω_0^e is applied on the purple electrode (refer to detailed view in Figure

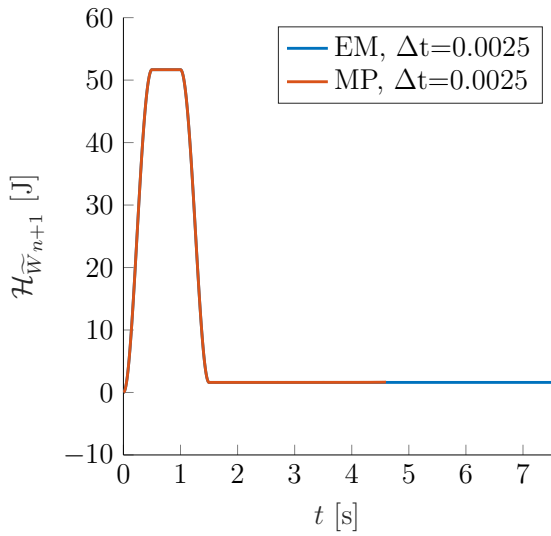


Figure 17: Numerical example 4. Time evolution of $\mathcal{H}_{\tilde{W}}$ with the proposed EM scheme and the midpoint-rule. Energy blow-up for midpoint-rule.

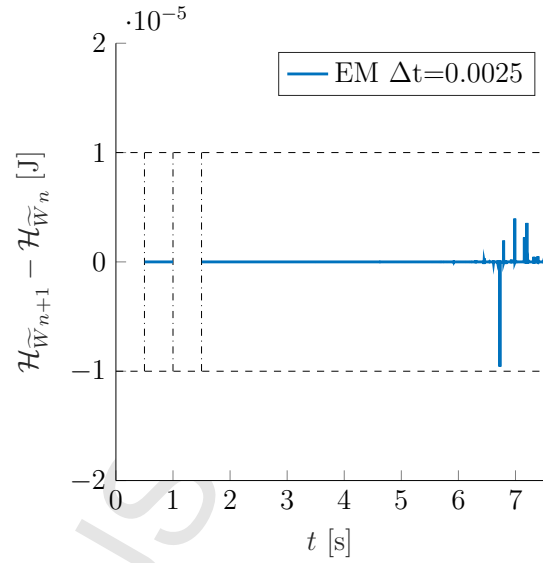


Figure 18: Numerical example 4. Time evolution of $\Delta \mathcal{H}_{\tilde{W}}$ in the time interval $[0.5, 1.5] \cup [1.5, 7.5]$ for hexahedral element with the proposed scheme.

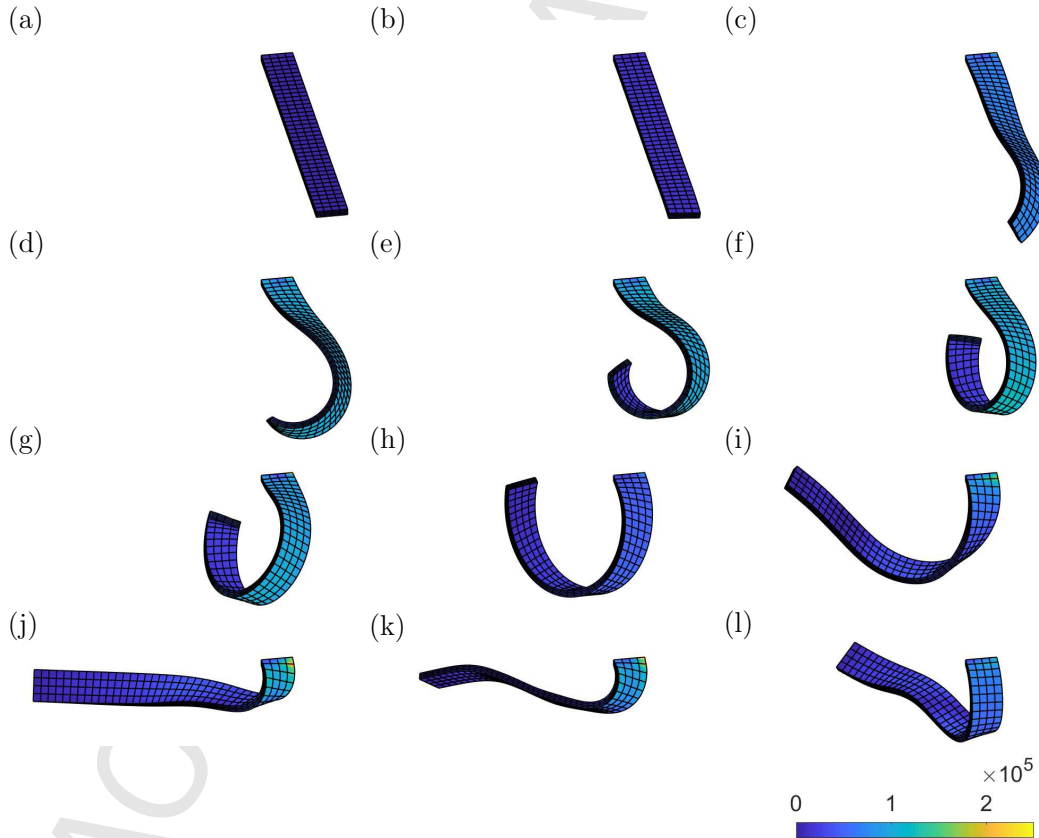


Figure 19: Numerical example 4. Contour plot of the von Mises stress for hexahedral element for different configurations corresponding to (left to right-top to bottom): (a) $t = 0$ s; (b) $t = 0.2$ s; (c) $t = 0.4$ s; (d) $t = 0.6$ s; (e) $t = 0.8$ s; (f) $t = 1$ s; (g) $t = 1.2$ s; (h) $t = 1.4$ s; (i) $t = 1.6$ s; (j) $t = 1.8$ s; (k) $t = 2$ s; (l) $t = 2.2$ s.

20) whereas a prescribed value of the electric potential of $\varphi = 0 V$ is applied on the blue electrode. The time dependent function ω_0^e is given by

$$\omega_0^e = (2 \times 10^{-3}) \times \begin{cases} \sin(\frac{0.5\pi}{1s} t) & \text{for } t \leq 1 \text{ s} \\ 1 & \text{for } t > 1 \text{ s} \end{cases} [Q/m^2]. \quad (80)$$

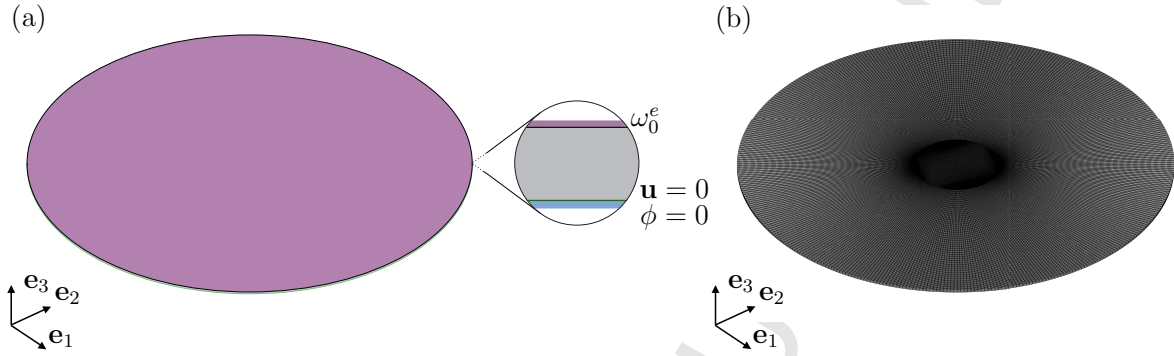
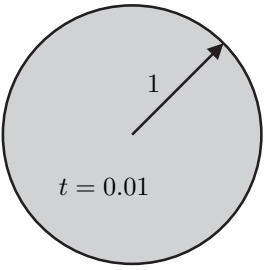


Figure 20: Numerical example 5. (a) Configuration and boundary conditions; (b) discretisation of one quarter considered: hexahedral mesh with $\{420639, 140213, 604800\}$ degrees of freedom for $\{\phi, \varphi, \mathbf{D}_0\}$. Interpolation spaces $Q2^C-Q2^C-Q1^D$.

The purely mechanical contribution of the constitutive model considered corresponds to that of a Mooney-Rivlin model (refer to equation (19)). The electromechanical component corresponds to that of an ideal dielectric elastomer (see equation (18)). The material parameters of the constitutive model can be found in Table 6.

Table 6: Numerical example 5. Material parameters, simulation parameters and geometry.

Mechanical parameters	μ_1	1×10^5	Pa	Geometry of the disc 
	μ_2	2×10^5	Pa	
	λ	1×10^5	Pa	
Electrical parameters	ϵ_0	8.854×10^{-12}	$A^2 s^4 kg^{-1} m^{-3}$	
	ϵ_r	4	N/V^2	
Ref. potential	ϕ_0	0	V	
Max. surface charge	ω_0	2×10^{-3}	Q/m^2	
Density	ρ_0	1000	$kg m^{-3}$	
Timestep size	Δt	0.01	s	
Simulation time	T	20	s	
Newton tolerance	ϵ	10^{-4}	J	

The discretisation shown in Figure 20_b has been used in this example. Specifically, a total of 25200 hexahedral $Q2^C-Q2^C-Q1^D$ finite elements for one quarter of the disc have been considered, yielding a total number of degrees of freedom (for one quarter) of $\{420639, 140213, 604800\}$ for the fields $\{\phi, \varphi, \mathbf{D}_0\}$.

Regarding objective **O5.I**, Figure 21 shows that the midpoint-rule time integrator exhibits an energy blow-up and becomes unstable approximately at the beginning of the time interval for which ω_0^e becomes constant. However, the proposed time integrator remains stable for the whole simulation for the same fixed time step size of $\Delta t = 0.01 s$. This example is particularly challenging, specially when using the midpoint-rule time integrator, as it can be observed from

the early energy blow-up just described. In addition, Figure 21 shows the evolution of $\mathcal{H}_{\widetilde{W}}$ for both the proposed EM time integrator and the midpoint-rule (before the latter becomes unstable). Crucially, $\mathcal{H}_{\widetilde{W}}$ remains constant when using the proposed EM scheme for the time interval $t > 1$ s, namely, when the surface charge ω_0^e in equation (80) remains constant, proving that the Hamiltonian is conserved in that range. This can be more clearly appreciated in Figure 22, where the variation $\Delta\mathcal{H}_{\widetilde{W}} = \mathcal{H}_{\widetilde{W}_{n+1}} - \mathcal{H}_{\widetilde{W}_n}$ is depicted for the aforementioned time interval. The maximum value of $|\Delta\mathcal{H}_{\widetilde{W}}|$ is always bounded below the user-defined Newton tolerance ϵ (refer to Table 6).

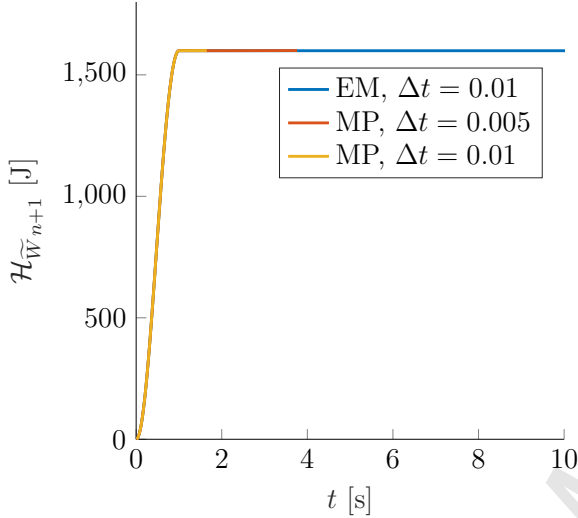


Figure 21: Numerical example 5. Time evolution of $\mathcal{H}_{\widetilde{W}}$ with the proposed EM scheme and the midpoint-rule. Energy blow-up for midpoint-rule.

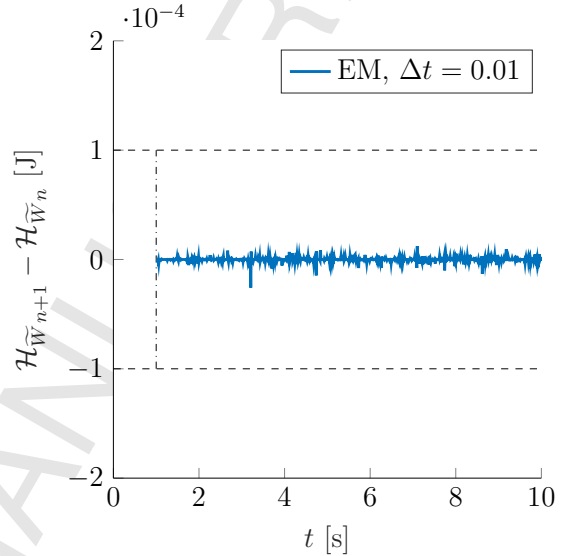


Figure 22: Numerical example 5. Time evolution of $\Delta\mathcal{H}_{\widetilde{W}}$ in the time interval $t > 1$ s for hexahedral element with the proposed scheme.

Finally, the contour plot distribution for the von Mises stress and the evolution of the electrically induced deformation in the actuator is depicted in Figure 23 for difference instances of time.

8. Conclusions

A new consistent energy-momentum one-step time integrator scheme is presented in the context of nonlinear electro-elastodynamics. Both a two-field Helmholtz's-based scheme and a three-field internal energy-based scheme have been developed. Following the work of Gil and Ortigosa [20, 37, 36], the internal energy functional is preferred in this paper over the Helmholtz energy functional for the definition of electromechanical constitutive models, due to considerations of material stability.

The new time integrator relies on the definition of four discrete derivative expressions of the internal energy, where each one represents the algorithmic counterpart of the work conjugates of the right Cauchy-Green deformation tensor, its co-factor, its determinant and the Lagrangian electric displacement field. Proof of thermodynamical consistency and of second order accuracy with respect to time of the resulting algorithm are presented. Finally, series of numerical examples have been included in order to prove the superior robustness and conservation properties of the (internal energy-based) EM time integration scheme proposed.

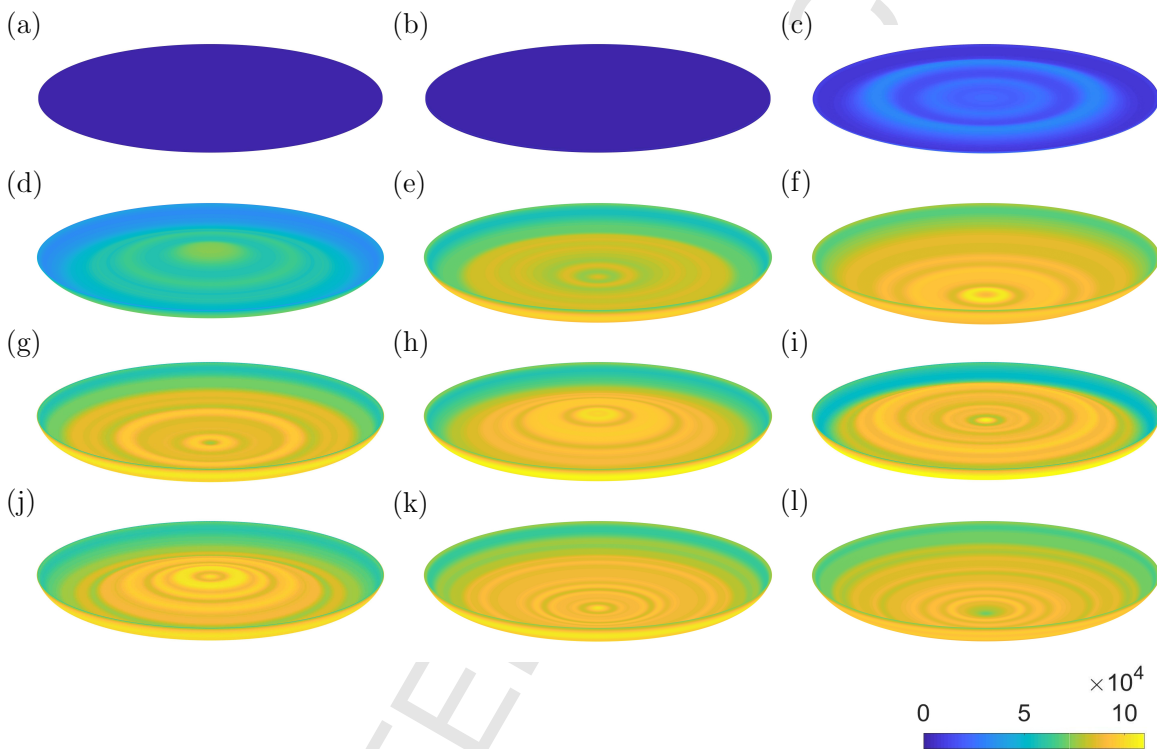


Figure 23: Numerical example 5. Contour plot of the von Mises stress for hexahedral element for different configurations corresponding to (left to right-top to bottom): (a) $t = 0$ s; (b) $t = 0.05$ s; (c) $t = 0.3$ s; (d) $t = 0.55$ s; (e) $t = 0.8$ s; (f) $t = 1.05$ s; (g) $t = 1.3$ s; (h) $t = 1.55$ s; (i) $t = 1.8$ s; (j) $t = 2.05$ s; (k) $t = 2.3$ s; (l) $t = 2.55$ s.

9. Acknowledgements

1 The first and fourth authors acknowledge the support provided by the Sêr Cymru National
2 Research Network under the Ser Cymru II Fellowship “Virtual engineering of the new generation of
3 biomimetic artificial muscles”, funded by the European Regional Development Fund. The third
4 and fifth authors acknowledge the support provided by the Deutsche Forschungsgemeinschaft
5 (DFG) under Grant BE 2285/9-2. The fourth author acknowledges the financial support received
6 through the European Training Network AdMoRe (Project ID: 675919).
7
8
9
10
11
12
13
14
15
16
17
18
19
20
21
22
23
24
25
26
27
28
29
30
31
32
33
34
35
36
37
38
39
40
41
42
43
44
45
46
47
48
49
50
51
52
53
54
55
56
57
58
59
60
61
62
63
64
65

Appendix A. Discrete derivatives of the internal energy

Appendix A.1. Definition of the discrete derivatives

Let us introduce the following notation, $\{\mathcal{V}_1, \mathcal{V}_2, \mathcal{V}_3, \mathcal{V}_4\} = \{\mathbf{C}, \mathbf{G}, C, \mathbf{D}_0\}$. This will facilitate the definition of the discrete derivatives $D_{\tilde{\mathcal{V}}_1} \tilde{W} = D_{\mathbf{C}} \tilde{W}$, $D_{\tilde{\mathcal{V}}_2} \tilde{W} = D_{\mathbf{G}} \tilde{W}$ and $D_{\tilde{\mathcal{V}}_3} \tilde{W} = D_C \tilde{W}$ in (48) and $D_{\tilde{\mathcal{V}}_4} \tilde{W} = D_{\mathbf{D}_0} \tilde{W}$ in (47)_d.

$$\begin{aligned} D_{\tilde{\mathcal{V}}_i} \tilde{W} &= \frac{1}{2} \left(D_{\tilde{\mathcal{V}}_{i,n+1,n}} \tilde{W} + D_{\tilde{\mathcal{V}}_{i,n,n+1}} \tilde{W} \right); & i \in Y = \{1, 2, 3, 4\}; \\ D_{\tilde{\mathcal{V}}_{i,n+1,n}} \tilde{W} &= D_{\tilde{\mathcal{V}}_i} \tilde{W} \left(\tilde{\mathcal{V}}_{i,n+1}, \tilde{\mathcal{V}}_{i,n} \right) \Big|_{\tilde{\mathcal{V}}_{j,n+1}, \tilde{\mathcal{V}}_{k,n}}; & \forall j \in Y : j < i; \forall k \in Y : k > i; \\ D_{\tilde{\mathcal{V}}_{i,n,n+1}} \tilde{W} &= D_{\tilde{\mathcal{V}}_i} \tilde{W} \left(\tilde{\mathcal{V}}_{i,n}, \tilde{\mathcal{V}}_{i,n+1} \right) \Big|_{\tilde{\mathcal{V}}_{j,n}, \tilde{\mathcal{V}}_{k,n+1}}; & \forall j \in Y : j < i; \forall k \in Y : k > i, \end{aligned} \quad (\text{A.1})$$

where the discrete operators $D_{\tilde{\mathcal{V}}_i} \tilde{W} \Big|_{\tilde{\mathcal{V}}_{j,n+1}, \tilde{\mathcal{V}}_{k,n}}$ and $D_{\tilde{\mathcal{V}}_i} \tilde{W} \Big|_{\tilde{\mathcal{V}}_{j,n}, \tilde{\mathcal{V}}_{k,n+1}}$ are defined as

$$\begin{aligned} D_{\tilde{\mathcal{V}}_i} \tilde{W} \Big|_{\tilde{\mathcal{V}}_{j,n+1}, \tilde{\mathcal{V}}_{k,n}} &= \partial_{\tilde{\mathcal{V}}_i} \tilde{W} \left(\tilde{\mathcal{V}}_{n+1/2} \right) \Big|_{\tilde{\mathcal{V}}_{j,n+1}, \tilde{\mathcal{V}}_{k,n}} \\ &\quad + \frac{\tilde{W} \left(\tilde{\mathcal{V}}_{n+1} \right) \Big|_{\tilde{\mathcal{V}}_{j,n+1}, \tilde{\mathcal{V}}_{k,n}} - \tilde{W} \left(\tilde{\mathcal{V}}_n \right) \Big|_{\tilde{\mathcal{V}}_{j,n+1}, \tilde{\mathcal{V}}_{k,n}} - \partial_{\tilde{\mathcal{V}}_i} \tilde{W} \left(\tilde{\mathcal{V}}_{n+1/2} \right) \Big|_{\tilde{\mathcal{V}}_{j,n+1}, \tilde{\mathcal{V}}_{k,n}} : \Delta \tilde{\mathcal{V}}_i}{\|\Delta \tilde{\mathcal{V}}_i\|^2} \Delta \tilde{\mathcal{V}}_i; \\ D_{\tilde{\mathcal{V}}_i} \tilde{W} \Big|_{\tilde{\mathcal{V}}_{j,n}, \tilde{\mathcal{V}}_{k,n+1}} &= \partial_{\tilde{\mathcal{V}}_i} \tilde{W} \left(\tilde{\mathcal{V}}_{n+1/2} \right) \Big|_{\tilde{\mathcal{V}}_{j,n}, \tilde{\mathcal{V}}_{k,n+1}} \\ &\quad + \frac{\tilde{W} \left(\tilde{\mathcal{V}}_{n+1} \right) \Big|_{\tilde{\mathcal{V}}_{j,n}, \tilde{\mathcal{V}}_{k,n+1}} - \tilde{W} \left(\tilde{\mathcal{V}}_n \right) \Big|_{\tilde{\mathcal{V}}_{j,n}, \tilde{\mathcal{V}}_{k,n+1}} - \partial_{\tilde{\mathcal{V}}_i} \tilde{W} \left(\tilde{\mathcal{V}}_{n+1/2} \right) \Big|_{\tilde{\mathcal{V}}_{j,n}, \tilde{\mathcal{V}}_{k,n+1}} : \Delta \tilde{\mathcal{V}}_i}{\|\Delta \tilde{\mathcal{V}}_i\|^2} \Delta \tilde{\mathcal{V}}_i. \end{aligned} \quad (\text{A.2})$$

From above equations (A.1) and (A.2), the directional derivative $D_{\mathbf{C}} \tilde{W}$ can be computed as

$$\begin{aligned} D_{\mathbf{C}} \tilde{W} &= \frac{1}{2} \left(\partial_{\mathbf{C}} \tilde{W} \left(\mathbf{C}_{n+1/2}, \mathbf{G}_{n+1}, C_{n+1}, \mathbf{D}_{0_{n+1}} \right) + \partial_{\mathbf{C}} \tilde{W} \left(\mathbf{C}_{n+1/2}, \mathbf{G}_n, C_n, \mathbf{D}_{0_n} \right) \right) \\ &\quad + \frac{1}{2} \frac{\tilde{W} \left(\mathbf{C}_{n+1}, \mathbf{G}_{n+1}, C_{n+1}, \mathbf{D}_{0_{n+1}} \right) - \tilde{W} \left(\mathbf{C}_n, \mathbf{G}_{n+1}, C_{n+1}, \mathbf{D}_{0_{n+1}} \right)}{\|\Delta \mathbf{C}\|^2} \Delta \mathbf{C} \\ &\quad + \frac{1}{2} \frac{\tilde{W} \left(\mathbf{C}_{n+1}, \mathbf{G}_n, C_n, \mathbf{D}_{0_n} \right) - \tilde{W} \left(\mathbf{C}_n, \mathbf{G}_n, C_n, \mathbf{D}_{0_n} \right)}{\|\Delta \mathbf{C}\|^2} \Delta \mathbf{C} \\ &\quad - \frac{1}{2} \frac{\partial_{\mathbf{C}} \tilde{W} \left(\mathbf{C}_{n+1/2}, \mathbf{G}_{n+1}, C_{n+1}, \mathbf{D}_{0_{n+1}} \right) : \Delta \mathbf{C}}{\|\Delta \mathbf{C}\|^2} \Delta \mathbf{C} \\ &\quad - \frac{1}{2} \frac{\partial_{\mathbf{C}} \tilde{W} \left(\mathbf{C}_{n+1/2}, \mathbf{G}_n, C_n, \mathbf{D}_{0_n} \right) : \Delta \mathbf{C}}{\|\Delta \mathbf{C}\|^2} \Delta \mathbf{C}. \end{aligned} \quad (\text{A.3})$$

Similarly, the directional derivative $D_{\mathbf{G}}\widetilde{W}$ can be computed as

$$\begin{aligned}
D_{\mathbf{G}}\widetilde{W} &= \frac{1}{2} \left(\partial_{\mathbf{G}}\widetilde{W}(\mathbf{C}_n, \mathbf{G}_{n+1/2}, C_{n+1}, \mathbf{D}_{0_{n+1}}) + \partial_{\mathbf{G}}\widetilde{W}(\mathbf{C}_{n+1}, \mathbf{G}_{n+1/2}, C_n, \mathbf{D}_{0_n}) \right) \\
&+ \frac{1}{2} \frac{\widetilde{W}(\mathbf{C}_n, \mathbf{G}_{n+1}, C_{n+1}, \mathbf{D}_{0_{n+1}}) - \widetilde{W}(\mathbf{C}_n, \mathbf{G}_n, C_{n+1}, \mathbf{D}_{0_{n+1}})}{\|\Delta\mathbf{G}\|^2} \Delta\mathbf{G} \\
&+ \frac{1}{2} \frac{\widetilde{W}(\mathbf{C}_{n+1}, \mathbf{G}_{n+1}, C_n, \mathbf{D}_{0_n}) - \widetilde{W}(\mathbf{C}_{n+1}, \mathbf{G}_n, C_n, \mathbf{D}_{0_n})}{\|\Delta\mathbf{G}\|^2} \Delta\mathbf{G} \\
&- \frac{1}{2} \frac{\partial_{\mathbf{G}}\widetilde{W}(\mathbf{C}_n, \mathbf{G}_{n+1/2}, C_{n+1}, \mathbf{D}_{0_{n+1}}) : \Delta\mathbf{G}}{\|\Delta\mathbf{G}\|^2} \Delta\mathbf{G} \\
&- \frac{1}{2} \frac{\partial_{\mathbf{G}}\widetilde{W}(\mathbf{C}_{n+1}, \mathbf{G}_{n+1/2}, C_n, \mathbf{D}_{0_n}) : \Delta\mathbf{G}}{\|\Delta\mathbf{G}\|^2} \Delta\mathbf{G}.
\end{aligned} \tag{A.4}$$

Furthermore, the directional derivative $D_{\mathbf{C}}\widetilde{W}$ can be computed as

$$\begin{aligned}
D_{\mathbf{C}}\widetilde{W} &= \frac{1}{2} \frac{\widetilde{W}(\mathbf{C}_n, \mathbf{G}_n, C_{n+1}, \mathbf{D}_{0_{n+1}}) - \widetilde{W}(\mathbf{C}_n, \mathbf{G}_n, C_n, \mathbf{D}_{0_{n+1}})}{\|\Delta\mathbf{C}\|} \\
&+ \frac{1}{2} \frac{\widetilde{W}(\mathbf{C}_{n+1}, \mathbf{G}_{n+1}, C_{n+1}, \mathbf{D}_{0_n}) - \widetilde{W}(\mathbf{C}_{n+1}, \mathbf{G}_{n+1}, C_n, \mathbf{D}_{0_n})}{\|\Delta\mathbf{C}\|}.
\end{aligned} \tag{A.5}$$

Finally, the directional derivative $D_{\mathbf{D}_0}\widetilde{W}$ can be computed as

$$\begin{aligned}
D_{\mathbf{D}_0}\widetilde{W} &= \frac{1}{2} \left(\partial_{\mathbf{D}_0}\widetilde{W}(\mathbf{C}_n, \mathbf{G}_n, C_n, \mathbf{D}_{0_{n+1/2}}) + \partial_{\mathbf{D}_0}\widetilde{W}(\mathbf{C}_{n+1}, \mathbf{G}_{n+1}, C_{n+1}, \mathbf{D}_{0_{n+1/2}}) \right) \\
&+ \frac{1}{2} \frac{\widetilde{W}(\mathbf{C}_n, \mathbf{G}_n, C_n, \mathbf{D}_{0_{n+1}}) - \widetilde{W}(\mathbf{C}_n, \mathbf{G}_n, C_n, \mathbf{D}_{0_n})}{\|\Delta\mathbf{D}_0\|^2} \Delta\mathbf{D}_0 \\
&+ \frac{1}{2} \frac{\widetilde{W}(\mathbf{C}_{n+1}, \mathbf{G}_{n+1}, C_{n+1}, \mathbf{D}_{0_{n+1}}) - \widetilde{W}(\mathbf{C}_{n+1}, \mathbf{G}_{n+1}, C_{n+1}, \mathbf{D}_{0_n})}{\|\Delta\mathbf{D}_0\|^2} \Delta\mathbf{D}_0 \\
&- \frac{1}{2} \frac{\partial_{\mathbf{D}_0}\widetilde{W}(\mathbf{C}_n, \mathbf{G}_n, C_n, \mathbf{D}_{0_{n+1/2}}) \cdot \Delta\mathbf{D}_0}{\|\Delta\mathbf{D}_0\|^2} \Delta\mathbf{D}_0 \\
&- \frac{1}{2} \frac{\partial_{\mathbf{D}_0}\widetilde{W}(\mathbf{C}_{n+1}, \mathbf{G}_{n+1}, C_{n+1}, \mathbf{D}_{0_{n+1/2}}) \cdot \Delta\mathbf{D}_0}{\|\Delta\mathbf{D}_0\|^2} \Delta\mathbf{D}_0.
\end{aligned} \tag{A.6}$$

Appendix A.2. Proof of directionality property

The objective of this section is to prove that the definition of the discrete derivatives of the internal energy $\widetilde{W}(\mathbf{C}, \mathbf{G}, C, \mathbf{D}_0)$ in (A.1) and (A.2) satisfy the directionality property in equation (49). For that, let us denote the expression on the left-hand side of the directionality property in (49) as \mathcal{T} , namely

$$\mathcal{T} = D_{\mathbf{C}}W : \Delta\mathbf{C} + D_{\mathbf{G}}W : \Delta\mathbf{G} + D_C W \Delta C + D_{\mathbf{D}_0}W \cdot \Delta\mathbf{D}_0. \tag{A.7}$$

Substitution of the expressions for $D_{\mathbf{C}}\widetilde{W}$ (A.3), $D_{\mathbf{G}}\widetilde{W}$ (A.4), $D_{\mathbf{C}}\widetilde{W}$ (A.5) and $D_{\mathbf{D}_0}\widetilde{W}$ (A.6)

into (A.7) leads to

$$\begin{aligned}
\mathcal{T} &= \frac{1}{2}\widetilde{W}(\mathbf{C}_{n+1}, \mathbf{G}_{n+1}, C_{n+1}, \mathbf{D}_{0_{n+1}}) - \frac{1}{2}\widetilde{W}(\mathbf{C}_n, \mathbf{G}_{n+1}, C_{n+1}, \mathbf{D}_{0_{n+1}}) \\
&+ \frac{1}{2}\widetilde{W}(\mathbf{C}_{n+1}, \mathbf{G}_n, C_n, \mathbf{D}_{0_n}) - \frac{1}{2}\widetilde{W}(\mathbf{C}_n, \mathbf{G}_n, C_n, \mathbf{D}_{0_n}) \\
&+ \frac{1}{2}\widetilde{W}(\mathbf{C}_n, \mathbf{G}_{n+1}, C_{n+1}, \mathbf{D}_{0_{n+1}}) - \frac{1}{2}\widetilde{W}(\mathbf{C}_n, \mathbf{G}_n, C_{n+1}, \mathbf{D}_{0_{n+1}}) \\
&+ \frac{1}{2}\widetilde{W}(\mathbf{C}_{n+1}, \mathbf{G}_{n+1}, C_n, \mathbf{D}_{0_n}) - \frac{1}{2}\widetilde{W}(\mathbf{C}_{n+1}, \mathbf{G}_n, C_n, \mathbf{D}_{0_n}) \\
&+ \frac{1}{2}\widetilde{W}(\mathbf{C}_n, \mathbf{G}_n, C_{n+1}, \mathbf{D}_{0_{n+1}}) - \frac{1}{2}\widetilde{W}(\mathbf{C}_n, \mathbf{G}_n, C_n, \mathbf{D}_{0_{n+1}}) \\
&+ \frac{1}{2}\widetilde{W}(\mathbf{C}_{n+1}, \mathbf{G}_{n+1}, C_{n+1}, \mathbf{D}_{0_n}) - \frac{1}{2}\widetilde{W}(\mathbf{C}_{n+1}, \mathbf{G}_{n+1}, C_n, \mathbf{D}_{0_n}) \\
&+ \frac{1}{2}\widetilde{W}(\mathbf{C}_n, \mathbf{G}_n, C_n, \mathbf{D}_{0_{n+1}}) - \frac{1}{2}\widetilde{W}(\mathbf{C}_n, \mathbf{G}_n, C_n, \mathbf{D}_{0_n}) \\
&+ \frac{1}{2}\widetilde{W}(\mathbf{C}_{n+1}, \mathbf{G}_{n+1}, C_{n+1}, \mathbf{D}_{0_{n+1}}) - \frac{1}{2}\widetilde{W}(\mathbf{C}_{n+1}, \mathbf{G}_{n+1}, C_{n+1}, \mathbf{D}_{0_n}) \\
&= \Delta\widetilde{W},
\end{aligned} \tag{A.8}$$

which proves that the definition of the discrete derivatives satisfy the directionality property.

Appendix A.3. Definition of the discrete derivatives in the limit

The objective of this section is to prove that the definition of the directional derivatives in equations (A.1) and (A.2) satisfies the second condition stated in Section 5.1.1, namely that they are well defined in the limit $\|\Delta\mathbf{C}\| \rightarrow 0$, $\|\Delta\mathbf{G}\| \rightarrow 0$, $\|\Delta C\| \rightarrow 0$ and $\|\Delta\mathbf{D}_0\| \rightarrow 0$. In particular, it will be proved in this Section that based on the definition of the discrete derivatives, these can be equivalently written as

$$D_{\widetilde{\mathbf{v}}_i}\widetilde{W} = \partial_{\widetilde{\mathbf{v}}_i}\widetilde{W}(\widetilde{\mathbf{v}}_{n+1/2}) + \sum_{i=1}^4 O(\|\Delta\widetilde{\mathbf{v}}_i\|^2) + \sum_{j=1, j \neq i}^4 \sum_{k=j+1, k \neq 1}^4 O(\|\Delta\widetilde{\mathbf{v}}_j\| \|\Delta\widetilde{\mathbf{v}}_k\|), \tag{A.9}$$

which would prove that they are well defined in the limit. For that, let us carry out a Taylor series expansion of the four different evaluations of the internal energy \widetilde{W} in equation (A.3) around

$\mathbf{C}_{n+1/2}$. This enables to express them as

$$\begin{aligned}
\widetilde{W}(\mathbf{C}_{n+1}, \mathbf{G}_{n+1}, C_{n+1}, \mathbf{D}_{0_{n+1}}) &= \widetilde{W}(\mathbf{C}_{n+1/2}, \mathbf{G}_{n+1}, C_{n+1}, \mathbf{D}_{0_{n+1}}) \\
&+ \partial_{\mathbf{C}} \widetilde{W}(\mathbf{C}_{n+1/2}, \mathbf{G}_{n+1}, C_{n+1}, \mathbf{D}_{0_{n+1}}) : \left(\frac{1}{2} \Delta \mathbf{C}\right) \\
&+ \left(\frac{1}{2} \Delta \mathbf{C}\right) : \partial_{\mathbf{C}\mathbf{C}}^2 \widetilde{W}(\mathbf{C}_{n+1/2}, \mathbf{G}_{n+1}, C_{n+1}, \mathbf{D}_{0_{n+1}}) : \left(\frac{1}{2} \Delta \mathbf{C}\right) + O(\|\Delta \mathbf{C}\|^3); \\
\widetilde{W}(\mathbf{C}_n, \mathbf{G}_{n+1}, C_{n+1}, \mathbf{D}_{0_{n+1}}) &= \widetilde{W}(\mathbf{C}_{n+1/2}, \mathbf{G}_{n+1}, C_{n+1}, \mathbf{D}_{0_{n+1}}) \\
&- \partial_{\mathbf{C}} \widetilde{W}(\mathbf{C}_{n+1/2}, \mathbf{G}_{n+1}, C_{n+1}, \mathbf{D}_{0_{n+1}}) : \left(\frac{1}{2} \Delta \mathbf{C}\right) \\
&+ \left(\frac{1}{2} \Delta \mathbf{C}\right) : \partial_{\mathbf{C}\mathbf{C}}^2 \widetilde{W}(\mathbf{C}_{n+1/2}, \mathbf{G}_{n+1}, C_{n+1}, \mathbf{D}_{0_{n+1}}) : \left(\frac{1}{2} \Delta \mathbf{C}\right) + O(\|\Delta \mathbf{C}\|^3); \\
\widetilde{W}(\mathbf{C}_{n+1}, \mathbf{G}_n, C_n, \mathbf{D}_{0_n}) &= \widetilde{W}(\mathbf{C}_{n+1/2}, \mathbf{G}_n, C_n, \mathbf{D}_{0_n}) \\
&+ \partial_{\mathbf{C}} \widetilde{W}(\mathbf{C}_{n+1/2}, \mathbf{G}_n, C_n, \mathbf{D}_{0_n}) : \left(\frac{1}{2} \Delta \mathbf{C}\right) \\
&+ \left(\frac{1}{2} \Delta \mathbf{C}\right) : \partial_{\mathbf{C}\mathbf{C}}^2 \widetilde{W}(\mathbf{C}_{n+1/2}, \mathbf{G}_n, C_n, \mathbf{D}_{0_n}) : \left(\frac{1}{2} \Delta \mathbf{C}\right) + O(\|\Delta \mathbf{C}\|^3); \\
\widetilde{W}(\mathbf{C}_n, \mathbf{G}_n, C_n, \mathbf{D}_{0_n}) &= \widetilde{W}(\mathbf{C}_{n+1/2}, \mathbf{G}_n, C_n, \mathbf{D}_{0_n}) \\
&- \partial_{\mathbf{C}} \widetilde{W}(\mathbf{C}_{n+1/2}, \mathbf{G}_n, C_n, \mathbf{D}_{0_n}) : \left(\frac{1}{2} \Delta \mathbf{C}\right) \\
&+ \left(\frac{1}{2} \Delta \mathbf{C}\right) : \partial_{\mathbf{C}\mathbf{C}}^2 \widetilde{W}(\mathbf{C}_{n+1/2}, \mathbf{G}_n, C_n, \mathbf{D}_{0_n}) : \left(\frac{1}{2} \Delta \mathbf{C}\right) + O(\|\Delta \mathbf{C}\|^3).
\end{aligned} \tag{A.10}$$

Introduction of above equation (A.10) into the last four terms on the right-hand side of equation (A.3) yields

$$\begin{aligned}
&\frac{1}{2} \frac{\widetilde{W}(\mathbf{C}_{n+1}, \mathbf{G}_{n+1}, C_{n+1}, \mathbf{D}_{0_{n+1}}) - \widetilde{W}(\mathbf{C}_n, \mathbf{G}_{n+1}, C_{n+1}, \mathbf{D}_{0_{n+1}})}{\|\Delta \mathbf{C}\|^2} \Delta \mathbf{C} \\
&+ \frac{1}{2} \frac{\widetilde{W}(\mathbf{C}_{n+1}, \mathbf{G}_n, C_n, \mathbf{D}_{0_n}) - \widetilde{W}(\mathbf{C}_n, \mathbf{G}_n, C_n, \mathbf{D}_{0_n})}{\|\Delta \mathbf{C}\|^2} \Delta \mathbf{C} \\
&- \frac{1}{2} \frac{\partial_{\mathbf{C}} \widetilde{W}(\mathbf{C}_{n+1/2}, \mathbf{G}_{n+1}, C_{n+1}, \mathbf{D}_{0_{n+1}}) : \Delta \mathbf{C}}{\|\Delta \mathbf{C}\|^2} \Delta \mathbf{C} \\
&- \frac{1}{2} \frac{\partial_{\mathbf{C}} \widetilde{W}(\mathbf{C}_{n+1/2}, \mathbf{G}_n, C_n, \mathbf{D}_{0_n}) : \Delta \mathbf{C}}{\|\Delta \mathbf{C}\|^2} \Delta \mathbf{C} = O(\|\Delta \mathbf{C}\|^2).
\end{aligned} \tag{A.11}$$

Introduction of the result in (A.11) into the expression for the directional derivative $D_{\mathbf{C}} \widetilde{W}$ in (13) leads to

$$D_{\mathbf{C}} \widetilde{W} = \frac{1}{2} \left(\partial_{\mathbf{C}} \widetilde{W}(\mathbf{C}_{n+1/2}, \mathbf{G}_{n+1}, C_{n+1}, \mathbf{D}_{0_{n+1}}) + \partial_{\mathbf{C}} \widetilde{W}(\mathbf{C}_{n+1/2}, \mathbf{G}_n, C_n, \mathbf{D}_{0_n}) \right) + O(\|\Delta \mathbf{C}\|^2). \tag{A.12}$$

A Taylor series expansion on the two first terms on the right-hand side of above equation

(A.12) enables these to be expressed as

$$\begin{aligned}
& \partial_C \widetilde{W}(\mathbf{C}_{n+1/2}, \mathbf{G}_{n+1}, C_{n+1}, \mathbf{D}_{0_{n+1}}) = \partial_C \widetilde{W}(\mathbf{C}_{n+1/2}, \mathbf{G}_{n+1/2}, C_{n+1/2}, \mathbf{D}_{0_{n+1/2}}) \\
& \quad + \partial_{\mathbf{C}\mathbf{G}}^2 \widetilde{W}(\mathbf{C}_{n+1/2}, \mathbf{G}_{n+1/2}, C_{n+1/2}, \mathbf{D}_{0_{n+1/2}}) : \left(\frac{1}{2} \Delta \mathbf{G}\right) \\
& \quad + \partial_{\mathbf{C}C}^2 \widetilde{W}(\mathbf{C}_{n+1/2}, \mathbf{G}_{n+1/2}, C_{n+1/2}, \mathbf{D}_{0_{n+1/2}}) \left(\frac{1}{2} \Delta C\right) \\
& \quad + \partial_{\mathbf{C}\mathbf{D}_0}^2 \widetilde{W}(\mathbf{C}_{n+1/2}, \mathbf{G}_{n+1/2}, C_{n+1/2}, \mathbf{D}_{0_{n+1/2}}) : \left(\frac{1}{2} \Delta \mathbf{D}_0\right) \\
& \quad + O(\|\Delta \mathbf{G}\|^2) + O(\Delta C^2) + O(\|\Delta \mathbf{D}_0\|^2) \\
& \quad + O(\|\Delta \mathbf{G}\| \Delta C) + O(\|\Delta \mathbf{G}\| \|\Delta \mathbf{D}_0\|) + O(\Delta C \|\Delta \mathbf{D}_0\|); \\
& \partial_C \widetilde{W}(\mathbf{C}_{n+1/2}, \mathbf{G}_n, C_n, \mathbf{D}_{0_n}) = \partial_C \widetilde{W}(\mathbf{C}_{n+1/2}, \mathbf{G}_{n+1/2}, C_{n+1/2}, \mathbf{D}_{0_{n+1/2}}) \\
& \quad - \partial_{\mathbf{C}\mathbf{G}}^2 \widetilde{W}(\mathbf{C}_{n+1/2}, \mathbf{G}_{n+1/2}, C_{n+1/2}, \mathbf{D}_{0_{n+1/2}}) : \left(\frac{1}{2} \Delta \mathbf{G}\right) \\
& \quad - \partial_{\mathbf{C}C}^2 \widetilde{W}(\mathbf{C}_{n+1/2}, \mathbf{G}_{n+1/2}, C_{n+1/2}, \mathbf{D}_{0_{n+1/2}}) \left(\frac{1}{2} \Delta C\right) \\
& \quad - \partial_{\mathbf{C}\mathbf{D}_0}^2 \widetilde{W}(\mathbf{C}_{n+1/2}, \mathbf{G}_{n+1/2}, C_{n+1/2}, \mathbf{D}_{0_{n+1/2}}) : \left(\frac{1}{2} \Delta \mathbf{D}_0\right) \\
& \quad + O(\|\Delta \mathbf{G}\|^2) + O(\Delta C^2) + O(\|\Delta \mathbf{D}_0\|^2) \\
& \quad + O(\|\Delta \mathbf{G}\| \Delta C) + O(\|\Delta \mathbf{G}\| \|\Delta \mathbf{D}_0\|) + O(\Delta C \|\Delta \mathbf{D}_0\|). \tag{A.13}
\end{aligned}$$

Introduction of (A.13) into (A.12) leads to the final expression for the discrete derivative $D_C \widetilde{W}$ (A.3) as

$$\begin{aligned}
D_C \widetilde{W} &= \partial_C \widetilde{W}(\mathbf{C}_{n+1/2}, \mathbf{G}_{n+1/2}, C_{n+1/2}, \mathbf{D}_{0_{n+1/2}}) \\
& \quad + O(\|\Delta \mathbf{C}\|^2) + O(\|\Delta \mathbf{G}\|^2) + O(\Delta C^2) + O(\|\Delta \mathbf{D}_0\|^2) \\
& \quad + O(\|\Delta \mathbf{G}\| \Delta C) + O(\|\Delta \mathbf{G}\| \|\Delta \mathbf{D}_0\|) + O(\Delta C \|\Delta \mathbf{D}_0\|), \tag{A.14}
\end{aligned}$$

which proves condition (A.9). Proceeding similarly, it would be possible to generalise above result (A.14) to the discrete derivatives $D_{\mathbf{G}} \widetilde{W}$ (A.4), $D_C \widetilde{W}$ (A.5) and $D_{\mathbf{D}_0} \widetilde{W}$ (A.6), namely

$$\begin{aligned}
D_{\mathbf{G}} \widetilde{W} &= \partial_{\mathbf{G}} \widetilde{W}(\mathbf{C}_{n+1/2}, \mathbf{G}_{n+1/2}, C_{n+1/2}, \mathbf{D}_{0_{n+1/2}}) \\
& \quad + O(\|\Delta \mathbf{C}\|^2) + O(\|\Delta \mathbf{G}\|^2) + O(\Delta C^2) + O(\|\Delta \mathbf{D}_0\|^2) \\
& \quad + O(\|\Delta \mathbf{C}\| \Delta C) + O(\|\Delta \mathbf{C}\| \|\Delta \mathbf{D}_0\|) + O(\Delta C \|\Delta \mathbf{D}_0\|); \\
D_C \widetilde{W} &= \partial_C \widetilde{W}(\mathbf{C}_{n+1/2}, \mathbf{G}_{n+1/2}, C_{n+1/2}, \mathbf{D}_{0_{n+1/2}}) \\
& \quad + O(\|\Delta \mathbf{C}\|^2) + O(\|\Delta \mathbf{G}\|^2) + O(\Delta C^2) + O(\|\Delta \mathbf{D}_0\|^2) \\
& \quad + O(\|\Delta \mathbf{C}\| \|\Delta \mathbf{G}\|) + O(\|\Delta \mathbf{C}\| \|\Delta \mathbf{D}_0\|) + O(\|\Delta \mathbf{G}\| \|\Delta \mathbf{D}_0\|); \tag{A.15} \\
D_{\mathbf{D}_0} \widetilde{W} &= \partial_{\mathbf{D}_0} \widetilde{W}(\mathbf{C}_{n+1/2}, \mathbf{G}_{n+1/2}, C_{n+1/2}, \mathbf{D}_{0_{n+1/2}}) \\
& \quad + O(\|\Delta \mathbf{C}\|^2) + O(\|\Delta \mathbf{G}\|^2) + O(\Delta C^2) + O(\|\Delta \mathbf{D}_0\|^2) \\
& \quad + O(\|\Delta \mathbf{C}\| \|\Delta \mathbf{G}\|) + O(\|\Delta \mathbf{C}\| \Delta C) + O(\|\Delta \mathbf{G}\| \Delta C).
\end{aligned}$$

- 1
2
3
4
5
6
7
8
9
10
11
12
13
14
15
16
17
18
19
20
21
22
23
24
25
26
27
28
29
30
31
32
33
34
35
36
37
38
39
40
41
42
43
44
45
46
47
48
49
50
51
52
53
54
55
56
57
58
59
60
61
62
63
64
65
- [1] J. M. Ball. Convexity conditions and existence theorems in nonlinear elasticity. *Archive for Rational Mechanics and Analysis*, 63(4):337–403, 1976.
 - [2] J. M. Ball. Energy-minimising configurations in nonlinear elasticity. *Archive for Rational Mechanics and Analysis*, 63(4):337–403, 1976.
 - [3] J. M. Ball. *Geometry, Mechanics and Dynamics*, chapter Some open problems in Elasticity, pages 3–59. Springer, 2002.
 - [4] K. J. Bathe. *Finite Element Procedures*. Prentice Hall, 1996.
 - [5] K. Bertoldi and M. Gei. Instabilities in multilayered soft dielectrics. *Journal of the Mechanics and Physics of Solids*, 59(1):18–42, 2011.
 - [6] P. Betsch, editor. *Structure-preserving Integrators in Nonlinear Structural Dynamics and Flexible Multibody Dynamics*, volume 565 of *CISM Courses and Lectures*. Springer-Verlag, 2016.
 - [7] P. Betsch and A. Janz. An energy-momentum consistent method for transient simulations with mixed finite elements developed in the framework of geometrically exact shells. *Int. J. Numer. Meth. Engng*, 108(5):423–455, 2016.
 - [8] P. Betsch, A. Janz, and C. Hesch. A Mixed Variational Framework for the Design of Energy-Momentum Schemes Relying on Polyconvex Stored Energy Functions. *Submitted to Comput. Methods Appl. Mech. Engrg*.
 - [9] J. Bonet, A. J. Gil, and R. Ortigosa. A computational framework for polyconvex large strain elasticity. *Computer Methods in Applied Mechanics and Engineering*, 283:1061–1094, 2015.
 - [10] J. Bonet, A. J. Gil, and R. Ortigosa. On a tensor cross product based formulation of large strain solid mechanics. *International Journal of Solids and Structures*, 84:49–63, 2016.
 - [11] J. Bonet, A. J. Gil, and R. D. Wood. *Nonlinear Continuum Mechanics for Finite Element Analysis: Statics*. Cambridge University Press, 2016.
 - [12] R. Bustamante. Transversely isotropic non-linear electro-active elastomers. *Acta Mechanica*, 206(3-4):237–259, 2009.
 - [13] R. Bustamante and J. Merodio. Constitutive structure in coupled non-linear electro-elasticity: Invariant descriptions and constitutive restrictions. *International Journal of Non-Linear Mechanics*, 46(10):1315 – 1323, 2011.
 - [14] S. Chiba, M. Waki, T. Wada, Y. Hirakawa, K. Masuda, and T. Ikoma. Consistent ocean wave energy harvesting using electroactive polymer (dielectric elastomer) artificial muscle generators. *Applied Energy*, 104(0):497–502, 2013.
 - [15] R. de Boer. *Vektor- und Tensorrechnung für Ingenieure*. Springer-Verlag, 1982.
 - [16] E.A. de Souza Neto, D. Perić, and D.R.J. Owen. *Computational Methods for Plasticity. Theory and Applications*. 2008.
 - [17] A. Dorfmann and R. W. Ogden. Nonlinear electroelasticity. *Acta Mechanica*, 174(3-4):167–183, 2005.
 - [18] A. Dorfmann and R.W. Ogden. Nonlinear electroelastic deformations. *Journal of Elasticity*, 82(2):99–127, 2006.

- 1
2
3
4
5
6
7
8
9
10
11
12
13
14
15
16
17
18
19
20
21
22
23
24
25
26
27
28
29
30
31
32
33
34
35
36
37
38
39
40
41
42
43
44
45
46
47
48
49
50
51
52
53
54
55
56
57
58
59
60
61
62
63
64
65
- [19] M. Franke, A. Janz, M. Schiebl, and P. Betsch. An energy-momentum consistent integration scheme using a polyconvexity-based framework for non-linear thermo-elastodynamics. *Submitted to Int. J. Numer. Meth. Engng.*
- [20] A. J. Gil and R. Ortigosa. A new framework for large strain electromechanics based on convex multi-variable strain energies: variational formulation and material characterisation. *Computer Methods in Applied Mechanics and Engineering*, 302:293–328, 2016.
- [21] O. Gonzalez. Exact energy and momentum conserving algorithms for general models in nonlinear elasticity. *Comput. Methods Appl. Mech. Engrg.*, 190:1763–1783, 2000.
- [22] O. Gonzalez and A. M. Stuart. *A first course in Continuum Mechanics*. Cambridge University Press, 2008.
- [23] M. Groß and P. Betsch. Energy-momentum consistent finite element discretization of dynamic finite viscoelasticity. *Int. J. Numer. Meth. Engng*, 81(11):1341–1386, 2010.
- [24] M. Gross, P. Betsch, and P. Steinmann. Conservation properties of a time FE method. Part IV: Higher order energy and momentum conserving schemes. *Int. J. Numer. Methods Eng.*, 63:1849–1897, 2005.
- [25] M. Groß and J. Dietzsch. Variational-based energy-momentum schemes of higher-order for elastic fiber-reinforced continua. *Comput. Methods Appl. Mech. Engrg.*, 283:1061–1094, 2015.
- [26] C. Hesch and P. Betsch. Energy-momentum consistent algorithms for dynamic thermomechanical problems – application to mortar domain decomposition problems. *Int. J. Numer. Meth. Engng*, 86(11):1277–1302, 2011.
- [27] M. Itskov and V. N. Khiêm. A polyconvex anisotropic free energy function for electro- and magneto-rheological elastomers. *Mathematics and Mechanics of Solids*, pages 1–12, 2014.
- [28] M. Jabareen. On the modeling of electromechanical coupling in electroactive polymers using the mixed finite element formulation. *Procedia {IUTAM}*, 12:105–115, 2015. {IUTAM} Symposium on Mechanics of Soft Active Materials.
- [29] G. Kofod, P. Sommer-Larsen, R. Kornbluh, and R. Pelrine. Actuation response of polyacrylate dielectric elastomers. *Journal of Intelligent Material Systems and Structures*, 14(12):787–793, 2003.
- [30] T. Li, C. Keplinger, R. Baumgartner, S. Bauer, W. Yang, and Z. Suo. Giant voltage-induced deformation in dielectric elastomers near the verge of snap-through instability. *Journal of the Mechanics and Physics of Solids*, 61(2):611–628, 2013.
- [31] J. E. Marsden and T. J. R. Hughes. *Mathematical foundations of elasticity*. 1994.
- [32] S. C. Martín and J. C. García Orden. On energy-entropy-momentum integration methods for discrete thermo-visco-elastodynamics. *Computers & Structures*, 181:3–20, 2017. UK Association of Computational Mechanics.
- [33] R. M. McMeeking and C. M. Landis. Electrostatic forces and stored energy for deformable dielectric materials. *Journal of Applied Mechanics*, 72(4):581–590, 2008.
- [34] C. Miehe, D. Vallicotti, and D. Zäh. Computational structural and material stability analysis in finite electro-elasto-statics of electro-active materials. *International Journal for Numerical Methods in Engineering*, 102(10):1605–1637, 2015. nme.4855.

- 1
2
3
4
5
6
7
8
9
10
11
12
13
14
15
16
17
18
19
20
21
22
23
24
25
26
27
28
29
30
31
32
33
34
35
36
37
38
39
40
41
42
43
44
45
46
47
48
49
50
51
52
53
54
55
56
57
58
59
60
61
62
63
64
65
- [35] A. O'Halloran, F. O'Malley, and P. McHugh. A review on dielectric elastomer actuators, technology, applications, and challenges. *Journal of Applied Physics*, 104(7), 2008.
- [36] R. Ortigosa and A. J. Gil. A new framework for large strain electromechanics based on convex multi-variable strain energies: Conservation laws, hyperbolicity and extension to electromagneto-mechanics. *Computer Methods in Applied Mechanics and Engineering*, 309:202–242, 2016.
- [37] R. Ortigosa and A. J. Gil. A new framework for large strain electromechanics based on convex multi-variable strain energies: Finite element discretisation and computational implementation. *Computer Methods in Applied Mechanics and Engineering*, 302:329–360, 2016.
- [38] R. Ortigosa and A. J. Gil. A computational framework for incompressible electromechanics based on convex multi-variable strain energies for geometrically exact shell theory. *Computer Methods in Applied Mechanics and Engineering*, 317:792–816, 2017.
- [39] R. Ortigosa, A. J. Gil, and C. H. Lee. A computational framework for large strain nearly and truly incompressible electromechanics based on convex multi-variable strain energies. *Computer Methods in Applied Mechanics and Engineering*, 310:297–334, 2016.
- [40] R. Pelrine, R. Kornbluh, Q. Pei, and J. Joseph. High-speed electrically actuated elastomers with strain greater than 100 %. *Science*, 287(5454):836–839, 2000.
- [41] R. E. Pelrine, R. D. Kornbluh, and J. P. Joseph. Electrostriction of polymer dielectrics with compliant electrodes as a means of actuation. *Sensors and Actuators A: Physical*, 64(1):77–85, 1998.
- [42] Ron Pelrine, Roy D. Kornbluh, Qibing Pei, Scott Stanford, Seajin Oh, Joseph Eckerle, Robert J. Full, Marcus A. Rosenthal, and Kenneth Meijer. Dielectric elastomer artificial muscle actuators: toward biomimetic motion, 2002.
- [43] R. Poya, A. J. Gil, R. Ortigosa, R. Sevilla, J. Bonet, and W. A. Wall. A curvilinear high order finite element framework for electromechanics: From linearised electro-elasticity to massively deformable dielectric elastomers. *Computer Methods in Applied Mechanics and Engineering*, 329:75–117, 2018.
- [44] I. Romero. An analysis of the stress formula for energy-momentum methods in nonlinear elastodynamics. *Computational Mechanics*, 50(5):603–610, Nov 2012.
- [45] J. Schröder, P. Wriggers, and D. Balzani. A new mixed finite element based on different approximations of the minors of deformation tensors. *Computer Methods in Applied Mechanics and Engineering*, 200(49-52):3583–3600, 2011.
- [46] M. H. Siboni, R. Avazmohammadi, and P. P. Castañeda. Electromechanical instabilities in fiber-constrained, dielectric-elastomer composites subjected to all-around dead-loading. *Mathematics and Mechanics of Solids*, 2014.
- [47] M. H. Siboni and P. P. Castañeda. Fiber-constrained, dielectric-elastomer composites: Finite-strain response and stability analysis. *Journal of the Mechanics and Physics of Solids*, 68(0):211–238, 2014.
- [48] J. C. Simo and N. Tarnow. The discrete energy-momentum method. conserving algorithms for nonlinear elastodynamics. *Zeitschrift für angewandte Mathematik und Physik ZAMP*, 43(5):757–792, Sep 1992.

- 1
2
3
4
5
6
7
8
9
10
11
12
13
14
15
16
17
18
19
20
21
22
23
24
25
26
27
28
29
30
31
32
33
34
35
36
37
38
39
40
41
42
43
44
45
46
47
48
49
50
51
52
53
54
55
56
57
58
59
60
61
62
63
64
65
- [49] S. Skatulla, C. Sansour, and A. Arockiarajan. A multiplicative approach for nonlinear electro-elasticity. *Computer Methods in Applied Mechanics and Engineering*, 245-246(0):243–255, 2012.
- [50] Z. Suo, X. Zhao, and W. H. Greene. A nonlinear field theory of deformable dielectrics. *Journal of the Mechanics and Physics of Solids*, 56(2):467–486, 2008.
- [51] F. Vogel, R. Bustamante, and P. Steinmann. On some mixed variational principles in electro-elasticostatics. *International Journal of Non-Linear Mechanics*, 47(2):341–354, 2012. Nonlinear Continuum Theories.
- [52] D. K. Vu and P. Steinmann. A 2-D coupled BEM-FEM simulation of electro-elasticostatics at large strain. *Computer Methods in Applied Mechanics and Engineering*, 199(17-20):1124–1133, 2010.
- [53] D. K. Vu and P. Steinmann. On 3-D coupled BEM-FEM simulation of nonlinear electro-elasticostatics. *Computer Methods in Applied Mechanics and Engineering*, 201-204(0):82–90, 2012.
- [54] D. K. Vu, P. Steinmann, and G. Possart. Numerical modelling of non-linear electroelasticity. *International Journal for Numerical Methods in Engineering*, 70(6):685–704, 2007.